https://doi.org/10.5194/egusphere-2026-5635
Preprint. Discussion started: 6 November 2026
© Author(s) 2026. CC BY 4.0 License.

GLAMODAT (v1.0): a model-data comparison tool for assessing transient palaeoglacier simulations

Andreas Henz[1], Sarah Kamleitner[1,2], Samuel U. Nussbaumer[1], Tancrède P.M. Leger[2], Guillaume Jouvet[2], and Andreas Vieli[1]

[1]Department of Geography, University of Zurich, Zurich, Switzerland
[2]Institute of Earth Surface Dynamics, University of Lausanne, Lausanne, Switzerland

Correspondence: Andreas Henz (andreas.henz@geo.uzh.ch)

Abstract. Current glacier model-data comparison methods often lack quantitative, automated validation for reconstructing complex palaeoglaciers and palaeo ice fields over millennia. Rigorous validation and automatic evaluation is critical for improving the reliability of glacier reconstructions and their use in understanding past climate and future projections. We introduce an open-source, Python-based comparison tool (GLAMODAT version 1.0) that automatically evaluates palaeoglacier model simulations against dated constraints on glacier history. GLAMODAT successfully quantifies model-data mismatches and demonstrates robustness in both synthetic and real-world case studies. It effectively tracks multiple phases of advance and retreat periods within mountain valleys. It is designed for validating single palaeoglacier simulations or entire ensembles by integrating weighted misfit scoring and adaptive parameter space exploration. It enables advancements in palaeoglacier reconstructions, climate reconstructions, and parameter studies in glacier modelling.

1 Introduction

Climate variation is the main forcing of glacier change. Hence, since the early days of glaciological research, glacier reconstructions have provided insights into past climate variability (Ahlmann, 1922; Sissons, 1974; Porter, 1975; Nesje and Dahl, 1992; Ohmura et al., 1992) while projections of glacier evolution under future climate change are critical for assessing its impacts such as water availability or natural hazards (Rounce et al., 2023; Jacquemart et al., 2024; Van Tricht et al., 2026; Frank et al., 2026). For both reconstructions and projections, glacier evolution modelling has proven to be an increasingly useful approach for understanding glacier behaviour and related climate conditions (Oerlemans, 2001; Mackintosh et al., 2017; Protin et al., 2019; Zekollari et al., 2025). Yet, ice-dynamical glacier evolution models are improving in their representation of physical processes and boundary conditions (e.g., thermal state, basal processes, mass balance). Consequently, they require an increasing amount of model parameters and input data, such as climate forcings (Marzeion et al., 2020; Rounce et al., 2020; Zekollari et al., 2022), which are even less clearly constrained in the past for palaeoglacier simulations. These model advances, however, combined with rising computational efficiency, now enable higher-resolution modelling, larger domains, longer timescales, and ensemble experiments, which are all valuable for palaeoglacier evolution modelling (Hock et al., 2019; Leger et al., 2025b; Henz et al., 2025). While such ensembles allow a more comprehensive assessment of model-based un-

https://doi.org/10.5194/egusphere-2026-5635
Preprint. Discussion started: 6 November 2026
© Author(s) 2026. CC BY 4.0 License.

certainties, the storage volume of model output and ensemble size grow substantially. The latter necessitates a rigorous and automated approach to evaluate the plausibility of simulations, enabling the identification of data-consistent palaeoglacier reconstructions (Napieralski, 2007; Ely et al., 2019; Albrecht et al., 2020; Lecavalier et al., 2023).

To assess the plausibility of palaeoglacier model simulations, empirical evidence from past glacier extents and their evolution through time is essential. An efficient and automated evaluation of glacier modelling output requires the related empirical evidence to be collated and quality-checked in a consistent format. Such a compilation of ages with corresponding locations and other geomorphological mappings became recently available for the European Alps with the AlpIce-1 database (Kamleitner et al., 2026b). The AlpIce-1 database fills a critical gap for the European Alps, inspired by similar initiatives for the former British-Irish Ice Sheet (BRITICE, Greenwood and Clark, 2008; Hughes et al., 2010, 2011; Clark et al., 2022), the Patagonian Ice Sheet (PATICE, Davies et al., 2020), the Greenland Ice Sheet (PaleoGrIS, Leger et al., 2024) and the Antarctic Ice Sheet (AntICEdat, Briggs and Tarasov, 2013; Lecavalier et al., 2023). AlpIce-1 compiles radiocarbon and terrestrial cosmogenic nuclide surface exposure ages, which indicate periods of ice-cover or ice-free conditions, as well as the positions and fluctuations of glacier margins across the entire European Alps between the Last Glacial Maximum (LGM) and the present day (Kamleitner et al., 2026b).

Previous glacier modelling reconstructions largely involved qualitative, manual comparisons between simulation outputs and geomorphological maps or ages (e.g., Oerlemans, 1997; Brown et al., 2013; Åkesson et al., 2017). For topographically confined ice flow such as Alpine glaciers, existing approaches include manual comparison of ice flow direction and ice thickness (Cohen et al., 2018) or manual to automatic comparison to glacier extent and ice thickness constraints for single time snapshots (Golledge et al., 2008; Jouvet et al., 2023; Leger et al., 2025b). Designed for larger ice sheets, existing model-data comparison approaches use empirically-based ice-margin chronologies (i.e., isochrones in interpretational maps) or can handle only a single ice sheet retreat or advance scenario (Tarasov and Peltier, 2004; Ely et al., 2019; Leger et al., 2025a). Other studies assess the quantitative fit of flow direction (Li et al., 2007; Napieralski, 2007) or proximity and form-comparison with mapped ice margins (Napieralski et al., 2006; Napieralski, 2007). All existing modelling reconstructions with model-data comparison that we are aware of typically rely on empirical data for single time slices, interpretive maps for temporal comparisons, or focus on individual retreat or advance phases. Our study presents a novel data-driven tool for automated model-data comparison, leveraging the availability of extensive empirical databases to enable analysis across millennial timescales and the complex, asynchronous histories of palaeoglacier dynamics for whole mountain ranges.

The advantage of directly using an empirical database in a model-data comparison approach is twofold: it builds on extensive and continuously growing data and it allows for seamless updates of these databases without requiring detailed re-interpretation. The glacier model-data comparison tool GLAMODAT has been developed using the newly compiled AlpIce-1 database (Kamleitner et al., 2026b) and palaeoglacier model simulations for the Younger Dryas (YD, 12.9–11.7 ka) to the Little Ice Age (LIA, 1250–1860 CE) period in the European Alps using the Instructed Glacier Model (IGM, Jouvet et al., 2021, 2026). However,

https://doi.org/10.5194/egusphere-2026-5635
Preprint. Discussion started: 6 November 2026
© Author(s) 2026. CC BY 4.0 License.

we designed GLAMODAT for compatibility with any other similar database and model output. The European Alps offer a rich yet fragmented picture of glacier fluctuations since the Last Glacial Maximum (LGM), leaving questions about deglaciation dynamics, Lateglacial transitions, and Holocene variability open (Ivy-Ochs et al., 2023a, b; Le Roy et al., 2024).

In the following sections, we describe the GLAMODAT model-data comparison tool in detail and demonstrate its capabilities and robustness by applying it in a synthetic case. In the synthetic case, the comparison tool uses glacier model simulations with real-world topography and geochronological data that are realistic but synthetically generated, as might be found in the European Alps. This step allows to illustrate and validate the performance of the tool under controlled conditions, ensuring its reliability before addressing real-world complexities. In addition, a demonstration of the application to a real-world case focusing on YD and Holocene glacier evolution in the Central Swiss Alps is presented in the Appendix.

2 GLAMODAT: An automated tool for palaeoglacier model-data comparison

2.1 Aim of the tool

GLAMODAT evaluates how well transient palaeoglacier model simulations fit chronological and geomorphological field evidence that constrain past glacier position. The spatial model-data misfit is quantified by calculating the geometric distance between the available dating location and the simulated ice extent (model output) within the corresponding time-window. A resulting final misfit score provides a metric for each simulation, supporting also options for automated adaptive exploration of the model parameter space.

For comparing model to data, GLAMODAT uses four palaeoglaciological context classes (aligned with AlpIce-1; Kamleitner et al., 2026b). It considers the fit of 'ages' at single locations and/or the fit for specific landforms with '(summary) event ages'. A match is obtained when the grid cell of the model matches the dating's age within it's uncertainty. Without a match, GLAMODAT searches in the model output for a near valid cell that matches within the age uncertainty and calculates the geometrical distance in between. The resulting distances are later used for computing misfit scores.

2.2 Geochronological and geomorphological input

The geochronological and geomorphological input provides the empirical foundation for constraining glacier model simulations. Any database with a compatible format may be used. The tool supports two types of input data:

- Individual ages: Single ages with associated age uncertainties and locations as a point dataset
- Event ages: Summary ages (incl. age uncertainties) assigned to a specific palaeoglacial event based on one or multiple individual ages. Event ages are linked to geomorphological features represented as points, lines, or polygons.

https://doi.org/10.5194/egusphere-2026-5635
Preprint. Discussion started: 6 November 2026
© Author(s) 2026. CC BY 4.0 License.

GLAMODAT handles the ages and event ages after their specific palaeoglaciological context (Fig. 1) following the same categorisation as in the AlpIce-1 database: *ice free*, *ice cover*, *ice margin*, and *bedrock exposure* (Kamleitner et al., 2026b). The following is what the contexts mean in relation to glacier model simulations during model-data comparison:

- Ice-free ages indicate locations that were ice free once during the age range defined by the dating and its uncertainty. This category also includes a temporal perspective, distinguishing between long-term deglaciation (ice free since) and short-term ice-free intervals, if later covered by ice.
- Ice-cover ages indicate long-term ice cover since at least then, derived from dated ice cores.
- Ice-margin ages represent known positions of glacier margins, such as erratic boulders deposited on moraine ridges. These ages are often associated with larger and mappable landforms such as terminal or lateral moraines (Fig. 1).
- Bedrock-exposure ages are obtained from in-situ bedrock surfaces and represent cumulative exposure durations. Under a simple exposure history, they can provide a minimum age for deglaciation, but complex exposure histories may result in ages that reflect cumulative exposure over multiple periods.

The comparison tool requires these compulsory category assignment for each dating to function, as the four categories must be treated differently (cf. Section 2.5). Except for the ice-margin context, ages are essentially one-sided constraints, meaning that ice-cover or ice-free conditions do indicate only the presence or absence of ice and not the distance to the ice margin. The empirical database must be provided as one or multiple shapefiles (.shp ending) and in the specific structure given in Table D1.

GLAMODAT can process not only single ages but also associated landforms (e.g. like the event age geometry shapefiles that are provided in AlpIce-1, Kamleitner et al., 2026b). This spatial representation improves the model-data comparison by allowing for direct validation using geomorphological mappings, thereby enlarging the spatial coverage of the constraints. The landforms are treated as event ages and must be provided including the same palaeo context categorisations like single ages including lower and upper age bounds (see input structure outlined in Table D1).

2.3 Glacier model requirements

We developed the glacier model-data comparison tool GLAMODAT to be compatible with outputs of the Instructed Glacier Model (IGM, Jouvet et al., 2021) as a forward glacier model, but other spatially-distributed glacier models can be used as long as they fulfil certain model requirements. First, GLAMODAT requires a regular rectangular mesh as model output (e.g. PISM, Bueler and Brown, 2009); if necessary, interpolation from non-rectangular meshes can be performed. Second, the glacier model must transiently simulate glacier evolution over millenial timescales to be useful for transient palaeoglacier reconstructions. Third, the glacier model output should have a spatial and temporal resolution comparable to the resolution of the database constraints. For example, if ages with different palaeoglaciological context are separated only several hundred meters also the

https://doi.org/10.5194/egusphere-2026-5635
Preprint. Discussion started: 6 November 2026
© Author(s) 2026. CC BY 4.0 License.

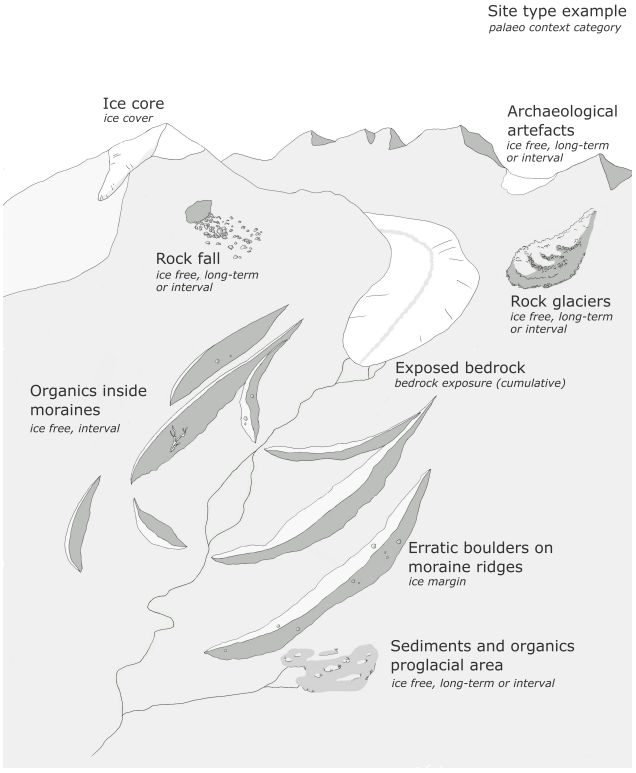


Figure 1. Schematic representation of geomorphological and geochronological empirical evidence used to constrain glacier models, including examples of landforms and their palaeoglaciological context (in italics). This illustration highlights key data sources, though not all possible data sources are shown; for a comprehensive overview, we refer to the AlpIce-1 database (Kamleitner et al., 2026b). Illustration: Alessia Fransioli.

glacier model should be able to resolve these fluctuation. Finally, the model must provide an output of glacier thickness or glacier surface together with basal topography, not only ice extent.

One key input for GLAMODAT are the two 2D model-data fields called "last ice cover" and "cumulative ice free", which record the time how long each grid cell is ice covered or ice free and the cumulative years a grid cell is ice free, respectively. The first data field is essential for comparing model results with observed ice-margin positions or known durations of ice-cover and ice-free ages, and the latter is used to compare with bedrock exposure ages. We illustrate the 2D data fields in the maps of Figs. 3, 4, and A5. Both data fields may be calculated either during the forward glacier simulations or from the stored model-output. Calculating them during the run captures short-term fluctuations at yearly resolution, whereas post-run calculations are limited to the frequency at which model data was saved. The code for both implementations in IGM and from IGM output is accessible via the link in the code availability section.

https://doi.org/10.5194/egusphere-2026-5635
Preprint. Discussion started: 6 November 2026
© Author(s) 2026. CC BY 4.0 License.

2.4 Workflow

GLAMODAT takes two inputs: a glacier simulation forward run and a structured database for model comparison. It then analyses each data entry (age or event age) inside the modelling domain in space and time, to identify how well the specific model run matches the ages (Fig. 2). A perfect match would mean the model output is correct in both time and location to explain this age. Not a full match results in two distances that are the horizontal and vertical distances to the next matching cell to the age or event age location. These distance values are the core of the comparison tool's output, saved as text file per age. The distance values can at the end of each model-data comparison be collated into a weighted final misfit score, using user-defined weights.

For each age or event age, the process follows a four-step procedure (A to D), as illustrated in Fig. 2. (A) First, the tool assesses whether the model output spatially aligns with the database entry. For this it allows to give a full match (zero distance) if the model fits the location and palaeoglaciological category once inside the uncertainty range of the dating, which is evaluated at the lower minimum of the uncertainty range (minimum age = youngest possible age). (B) Then, GLAMODAT additionally checks whether the model output matches the database entry later in the simulation. This is done for the categories ice free (long-term ice free) and ice margin, which locations should not again be ice-covered later then the age uncertainty and vice versa for ice cover categories, which locations should not be ice free later. If no match is found for the evaluated time step, in step (C) GLAMODAT searches for a near model grid cell that satisfies the criteria at the time of the dating, in a way that is explained in detail in Section 2.5. In the final step (D), GLAMODAT assigns a horizontal and vertical distance of mismatch to each age or event age. A perfect match results in a distance of 0 m, while a mismatch is quantified by the geometric distance (in meters) to the nearest matching cell. If no matching cell is found, GLAMODAT assigns a penalty value of the maximal search radius. If the event age has a spatial extension (lines, polygons), GLAMODAT generates points distanced in the simulation grid spacing or larger (max 10 points per landform) and treats all points separately (running step A to C) which are subsequently averaged to event age distances in step D for this landform. The calculated horizontal and vertical distances are individual measures for each age or event age. However, we provide additional to the comparison tool the option and code to combine them to a final mismatch score (Section 2.6) and present the options to use the distances in our applications (Sections 3 and A).

2.5 Treatment of different palaeoglacier contexts

2.5.1 Ice-margin context

To assess the fit of the glacier model simulations with dated ice margins, we require the (modelled) glacier margin to be at age or landform position within the temporal uncertainty range of the age or event age. A match is achieved when the dated feature and the model's ice margin coincide both spatially and temporally. If no such match is found, the tool expands the search for a near grid cell that satisfies the temporal criteria.

https://doi.org/10.5194/egusphere-2026-5635
Preprint. Discussion started: 6 November 2026
© Author(s) 2026. CC BY 4.0 License.

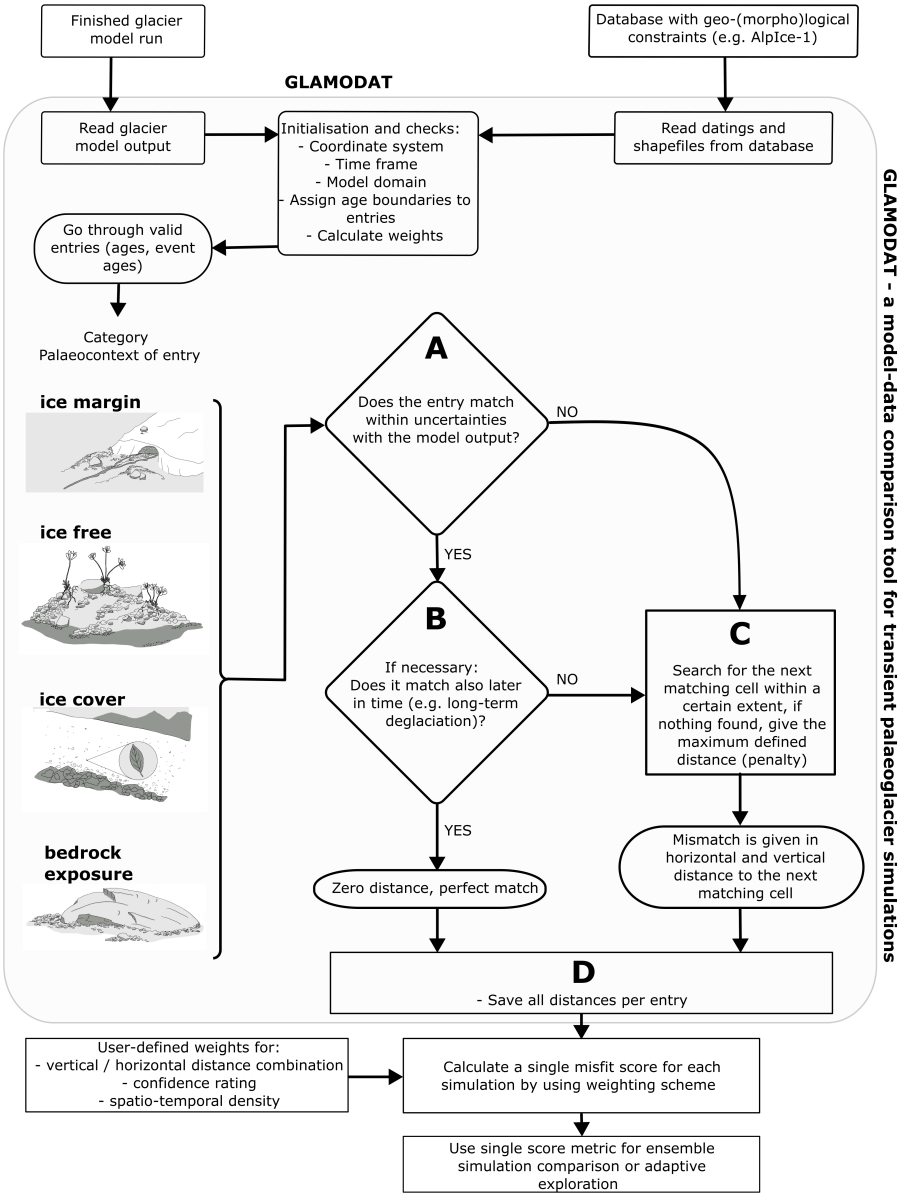


Figure 2. Schematic workflow of the glacier model-data comparison tool GLAMODAT. After initialisation, the tool processes each entry(single ages, event ages, or landforms with assigned event ages) through four steps: (A) calculate match of model output to point data; (B) re-evaluating for later ice cover or absence; (C) if not matching, searching iteratively for the next matching cell; and (D) attributing horizontal and vertical distances to each entry. These distances can be used for adaptive parameter exploration or analysed individually for deeper insights. Steps (A)–(C) vary slightly based on the palaeoglaciological context (Section 2.5). Drawings: Alessia Fransioli.

https://doi.org/10.5194/egusphere-2026-5635
Preprint. Discussion started: 6 November 2026
© Author(s) 2026. CC BY 4.0 License.

Finding the nearest matching ice margin is not always straightforward and depends on the age category. For example, landforms and dating results in an ice-margin context on a valley side often indicate peak thicknesses for a valley glacier. In such cases, if the modelled glacier is too small, the nearest ice margin likely lies at a lower elevation. In contrast, in the case of a dated terminal moraine of a glacier, the nearest ice margin lies in higher elevations if the glacier is too small but not on the side but usually in the back of the valley. To determine the direction in which to search for the next matching cell, GLAMODAT computes the gradient of the glaciation history using the "last ice cover" 2D data field (see Section 2.3) of either combined multiple model simulations (with an ensemble run) or selected simulations (Fig. C1). Using this "direction of deglaciation", the tool follows a specific path to find the next matching cell for every age, meaning we are searching for a matching cell in the right context and do not simply search radially for the next matching cell.

2.5.2 Ice-free context

The ice-free ages and ice-free event ages are evaluated by ensuring that the corresponding grid cell was ice free at least once inside the respective uncertainty range. For ice-free ages that indicate a long-term deglaciation (e.g., dated landform showing ice-free conditions since then) require the tool to check also model output beyond the age uncertainty, which means the cell is also checked for later ice cover (step B in Fig. 2). If the model does not match the ice-free condition at a given location, the tool searches for a nearby grid cell that meets the ice-free criteria. The tool follows the same process as described in section 2.5.1, in the direction towards less extensive ice cover.

2.5.3 Ice-cover context

For ice-cover ages, the model requires the grid cell to remain continuously ice covered since this age. If the model fails to meet this condition, the tool searches for a near grid cell that satisfies the ice cover requirement towards the direction of more extensive ice cover.

2.5.4 Bedrock-exposure context

Cumulative exposure-time ages indicate the duration a grid cell should remain ice free. GLAMODAT evaluates these ages by comparing the total ice-free period (using the cummulative ice free data field) to the minimum ice-free duration of the dating. A perfect match results in a zero-distance score; otherwise, the tool searches for the nearest grid cell that fits the criteria in direction of less extensive ice cover. Only model runs covering the entire period until after the LIA are considered for bedrock-exposure ages as the entire glaciation history is needed for a cumulative exposure dating.

2.6 Calculation of model-data mismatch - final misfit score calculation

Central to the automated model-data comparison for a large set of simulations is an final misfit score to compare all simulations between each other. GLAMODAT in a first instance calculates individual horizontal and vertical distances for single ages or event ages. We name the single value resulting from the collation of all individual distances the "final misfit score", which is

https://doi.org/10.5194/egusphere-2026-5635
Preprint. Discussion started: 6 November 2026
© Author(s) 2026. CC BY 4.0 License.

an objective measure of how well the model and data match overall. This final misfit score is calculated based on user-defined weights for the individual misfit-distances.

The first step in getting to a final misfit score is for GLAMODAT to combine the horizontal and vertical distances into one distance in 3D. However, a 1 km horizontal mismatch for glacier length in a flat valley may be more acceptable than a 500 m vertical mismatch in ice thickness for a lateral moraine. Therefore, we implement a weight to the vertical mismatch distance compared to the horizontal mismatch distance following this formula:

$$d = \sqrt{(\Delta x)^2 + (w_z \cdot \Delta z)^2} \tag{1}$$

where Δx represents the horizontal distance and Δz the vertical distance between the age location and the nearest fitting model grid-cell and w_z the weight to the vertical mismatch. Note that if the chosen weight is not equal to 1, the distance is no longer an Euclidean distance. This is why we call this a weighted distance or, when multiple ages are combined, a misfit score.

In a second step, GLAMODAT uses the calculated weighted distances to compute the final misfit score. For this two optional weighting schemes can be applied independently or in combination:

- Confidence rating weights account for the reliability of individual ages or event ages (high, medium, or low). For example, users might assign weights like 1, 1, 0 to high, medium, and low confidence ages, respectively. If no confidence rating is assigned in the data input, the GLAMODAT does not apply this weighting scheme.
- Spatio-temporal weighting adjusts the importance of each dating or event based on data density. If enabled, ages in areas or periods with abundant data are down-weighted to prevent dominance, while rare or isolated ages receive higher weights to maintain their significance. Users can control the strength of this weighting with a scaling factor (e.g., a factor of 1 means no adjustment, while a factor of 2 allows weights to vary maximum by a ratio of 1:2).

While recommended and default values are provided, users are free to define their own weighting schemes. GLAMODAT saves individual distances per age or event age, allowing for custom metrics if desired.

2.7 Adaptive parameter space exploration

GLAMODAT can optionally be employed to perform automated exploration and optimisation of the model parameter space for forward simulations, with the objective of minimising the final misfit score. This is achieved through real-time model-data comparison using GLAMODAT after each finished glacier simulation, yielding the quantitative final misfit scores to inform adaptive sampling algorithms. A variety of adaptive parameter space exploration algorithms exist, each characterised by distinct strengths and limitations, particularly with respect to the dimensionality of the parameter space, the independence of variables, and the nature of the parameters (continuous, discrete, or categorical). We demonstrate this capability in the case study presented in the Appendix, utilizing a Random Forest Optimization approach, for which the implementation is distributed as a separate python file alongside the comparison tool (Section A).

https://doi.org/10.5194/egusphere-2026-5635
Preprint. Discussion started: 6 November 2026
© Author(s) 2026. CC BY 4.0 License.

3 Application

3.1 Younger Dryas and Holocene glaciation in the Alps

The tool was tested and applied to the glaciation history spanning the Younger Dryas (YD) through the Holocene to the Little Ice Age (LIA). To this end, a synthetic case based on possible data from a catchment area in the Alps (see below) and a real-world case from the Central Swiss Alps (see Appendix) are used. The YD (12.9-11.7 ka) marks the last major glacier readvance of the Lateglacial in the Alps (Ivy-Ochs et al., 2023b; Binaghi et al., 2025), which succeeded the warmer Bølling–Allerød Interstadial. During the YD, glaciers re-advanced substantially and typically reached beyond their LIA extents (Binaghi et al., 2025). The successive Holocene featured a thermal maximum in the Early Holocene (11.7 ka to about 5 ka) followed by a general summer cooling trend towards the LIA (Ivy-Ochs et al., 2009; Affolter et al., 2019; Bette Otto-Bliesner et al., 2024), which represents the coldest period of the last about 8000 years (Wanner et al., 2022). Despite this generally warm phase, colder pulses, such as the 8.2 ka event, still caused substantial glacier advances (Alley et al., 1997; von Scheffer et al., 2025).

3.2 Glacier model for the test environment

For our application, we use the Instructed Glacier Model (IGM, Jouvet et al., 2021, 2026), a high-order ice mechanics model capable of computationally efficient glacier evolution simulations. Due to its efficiency and 3D glacier modelling, IGM is particularly well-suited for high-resolution, millennial-scale modelling over complex topographies. For this study, we enhanced IGM with an advanced surface mass balance module, detailed in Section B. This configuration ensures that IGM meets the model-data comparison requirements: sufficient resolution to capture field-scale geological details and the computational efficiency to run high-resolution ensemble simulations.

3.3 Input and synthetic age generation

To ease the interpretation of the output of the comparison tool, we illustrate its capabilities using a synthetic glacier model history based on a real-world valley (Brunnital, Central Switzerland, N 46.75, E 8.80) combined with plausible but generated ages of different palaeoglaciological categories as described above. Each glacier simulation is initialised with bedrock topography from the ALOS World 3D 30 m (AW3D30) digital elevation model (Japan Aerospace Exploration Agency, 2021) with subtracted present-day estimated ice thickness from Cook et al. (2023). Initial starting ice geometry is obtained by a steady state geometry matching the LIA glacier extent (Henz et al., 2025). As climate input, we use the statistically downscaled global climate model history with 1 km grid resolution (CHELSA TRaCE21k, 21-0 ka, Karger et al., 2020, 2023) in a timeframe from before the YD (about 15 ka) to 2000 CE.

We construct a reference experiment (A) by running the model forward for the given climate history. Two additional runs (B and C) test elevated and reduced temperatures by +0.25 K and -0.5 degrees, respectively (Table 1). The synthetic ages

https://doi.org/10.5194/egusphere-2026-5635
Preprint. Discussion started: 6 November 2026
© Author(s) 2026. CC BY 4.0 License.

Table 1. Three experiments are conducted to test the tool on a synthetic age data set. All experiments use the same region in central Switzerland (Brunnigletscher, Brunnital), with synthetic ages generated to perfectly match the glacier history of experiment A. After running the comparison tool, we calculate the average distance from each dating to the nearest matching grid cell in the glacier model output. Additionally, we count the number of ages and event ages that result in a full match.

Name	Climate input	change to experiment A	average distance to matching cell	10x elevation and weighted distance	number of fully matching ages (total: 10)
Experiment A	Karger et al. (2020) with temperature offset -0.5 K	-	0 m	0 m	10
Experiment B	Karger et al. (2020) with temperature offset -0.25 K	+ 0.25 K	549 m	1078 m	4
Experiment C	Karger et al. (2020) with temperature offset -1.0 K	- 0.5 K	293 m	486 m	5

database aligns perfectly with experiment A's glacier history, allowing controlled evaluation of GLAMODAT's performance. To simplify illustration, the synthetic ages are placed along the glacier's centre flowline (Fig. 3 a), but are spread temporally and spatially over the modelling domain. The ten generated ages cover all palaeoglaciological context categories.

3.4 Synthetic test result interpretations

The three different model runs (three different climate forcings) for the Brunnital result in three differing glacier evolution histories for the period from the YD to after the LIA period (ca. 14000 years of simulation). The length history shows for all three simulations largest extent in the YD (around 12 ka) and subsequent smallest extent just after the YD at around 11 ka. After that, the glacier extent fluctuates at low amplitude until it starts to expand slightly towards the LIA from around 7 ka onwards (Fig. 4).

For the reference run (experiment A), GLAMODAT correctly assigns a zero misfit distance to all synthetically generated ages, as indicated by the horizontal and vertical distances in Figure 4 and Table 1. In the cases of higher (or lower) temperatures and shorter (or longer) glaciers, some ages still match while others clearly disagree (Fig. 4 b and c). Matching ages despite altered climate input persist for several reasons: (1) the age is an ice-free indicator, and even with glaciers that are too short, it still fulfils this conditions of glacier history; (2) the age indicates ice cover, and with longer glaciers, this ice cover remains correct; and (3) the correct position (e.g., ice margin) falls within the age uncertainty bounds of the dating, which the tool still accepts as an acceptable match. All glacier length histories and attributed distances to the ages are presented in Fig. 4 a–c.

With this synthetic case, we demonstrate the use of the comparison tool, as it correctly associates a full match for the model run from which the synthetic data were generated. Furthermore, GLAMODAT identifies mismatches for the other runs where the glacier extent does not agree with all the ages and quantifies the misfit. For example, in experiment B (warmer), ice-free ages match while ice-cover and ice-margin ages do not match which indicates that glaciers in this experiment are not extensive enough. Similarly, in experiment C (colder), the observation that ice-cover ages match but ice-free ages are later overrun indicates that the ice cover in this model run is too extensive compared to the data. Looking at these single age mismatches tell us which experiment produces at these times too extensive ice cover and which underestimate it. Continuing from this, we

https://doi.org/10.5194/egusphere-2026-5635
Preprint. Discussion started: 6 November 2026
© Author(s) 2026. CC BY 4.0 License.

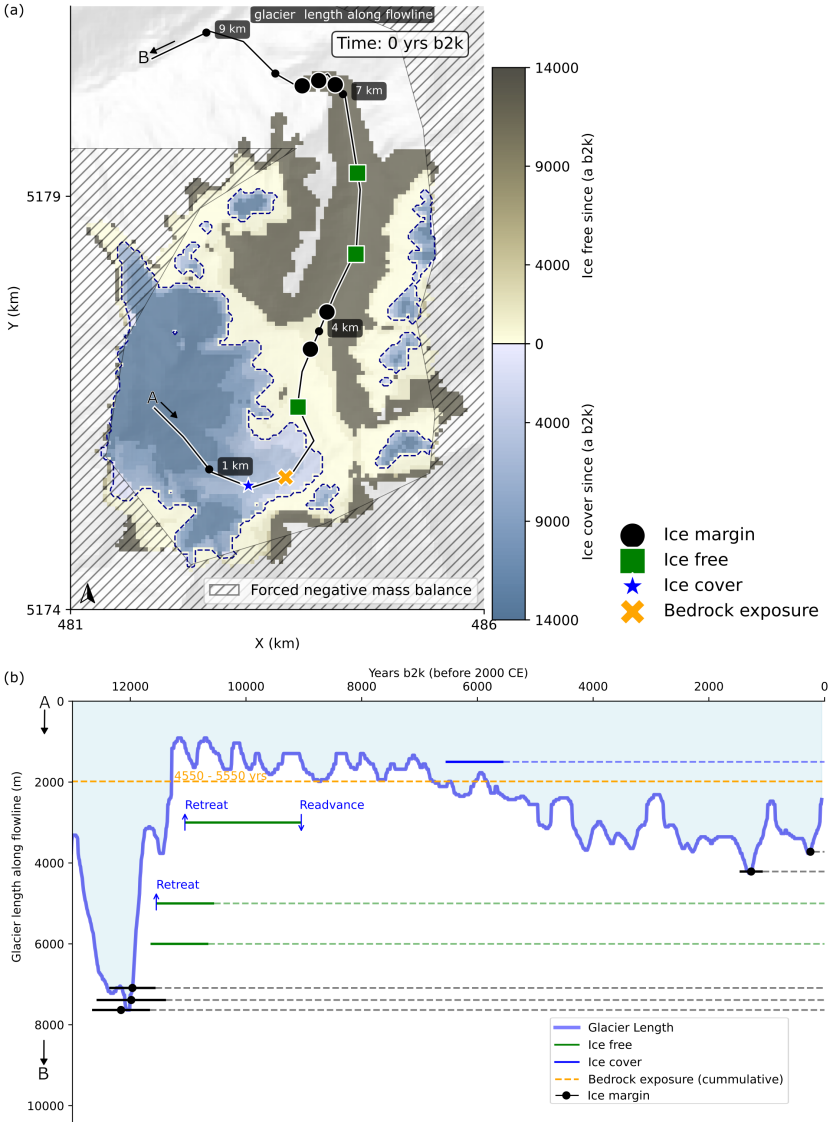


Figure 3. Modelled glacier extent and history and related synthetic ages of experiment A. (a) Map of modelled glacier history at a specific time step (2000 CE). The colour map illustrates the "last ice cover" 2D data field, showing either the time since ice retreat (brownish-greenish colours) or the duration of continuous ice cover (bluish colours) at the selected time step. This matrix is used to identify mismatches of the ice-margin, ice-free, and ice-cover contexts. The flowline is shown, on which all synthetic ages of different categories have been positioned. (b) Glacier length history along the flowline (see (a)), showing synthetic ages (corresponding symbols from (a)) with their uncertainty ranges. The dashed horizontal lines mark periods where ages have implications up to the present day; for example, a long-term ice-free age should never be ice covered again.

https://doi.org/10.5194/egusphere-2026-5635
Preprint. Discussion started: 6 November 2026
© Author(s) 2026. CC BY 4.0 License.

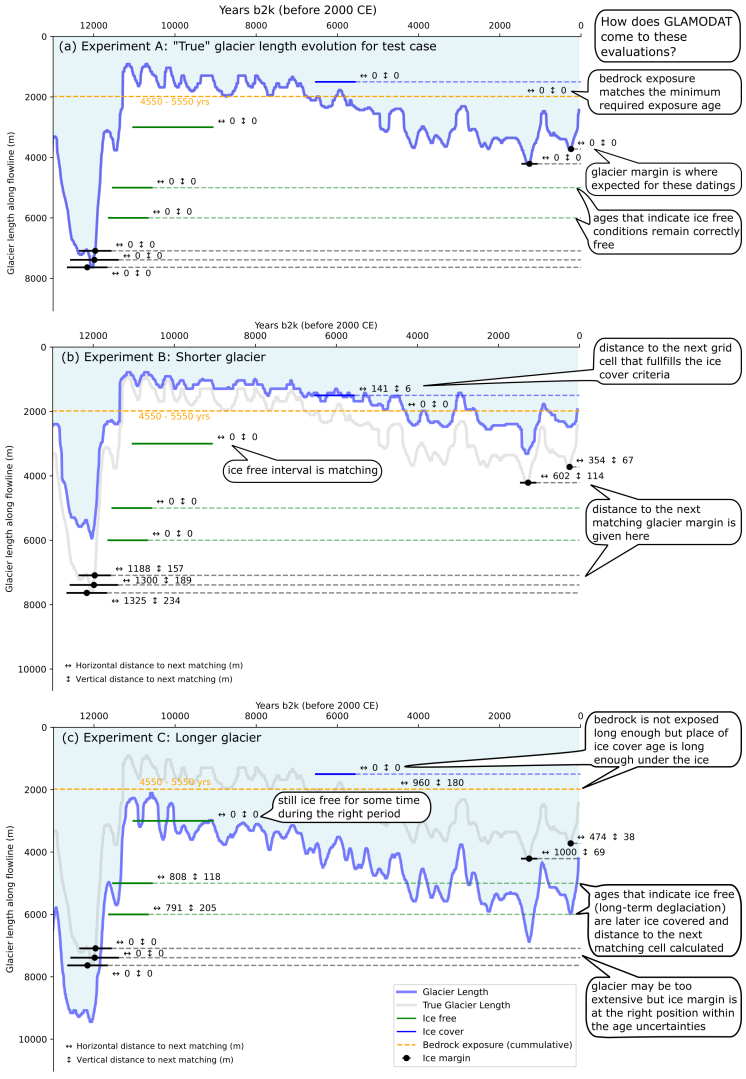


Figure 4. Visualisation of GLAMODAT's performance for the three test cases using age constraints and transiently modelled glacier output. (a) In experiment A (reference), the glacier model matches the synthetically generated landform ages perfectly. A map-view glacier history of this experiment is depicted in Fig C2. (b) In experiment B (warmer), the glaciers are too short, causing mismatches for ages indicating maximum ice positions or minimum ice-cover duration. Ice-free ages remain unaffected, as they are correctly ice free. (c) In experiment C (colder), the glaciers are too extensive, causing mismatch in ice-free ages and bedrock exposure ages as well as some ice-margin position. Some ages like ice cover still match, as the the model shows ice cover for the correct duration.

could now combine the single distances to an final misfit score, which allows automatic searching for best simulations. We demonstrate this ability in the real-world case study in Section A.

https://doi.org/10.5194/egusphere-2026-5635
Preprint. Discussion started: 6 November 2026
© Author(s) 2026. CC BY 4.0 License.

4 Discussion of comparison tool

The glacier model-data comparison tool, GLAMODAT, provides a robust quantitative framework for diagnosing mismatches between palaeoglacier model simulations and empirical data, but its effectiveness depends on critical design choices. One such choice is the method for identifying the next matching grid cell, which becomes non-trivial when moving beyond simple radial searches. Radial searches risk finding matching cells belonging to neighboring glaciers, leading to incorrect matches. To address this, GLAMODAT employs a glacier history map to ensure the search is constrained to the correct contextual path (Fig. C1). While this approach mitigates the risk of misattribution, it may introduce challenges in regions with complex glacier advance and retreat patterns. We are confident this method improves upon radial searches, as illustrated in Fig. C1. For example, the search path for the lowest ice margins (in the North in Fig. C1) correctly follows the valley floor upwards where the glacier originated. In contrast, a radial search would incorrectly match a closer, but contextually irrelevant, peak to the Southeast. Similarly, for the southern bedrock exposure age, a radial search would mistakenly select a closer matching cell to the South, ignoring the actual direction of glacier flow towards West and turning North.

GLAMODAT was designed to match a specific input structure of the geo(morpho)logical and geochronological data that must fit the required format (Tab D1). While the four distinct palaeoglaciological categories (including time perspectives long-term deglaciation and ice-free interval for ice-free conditions) cover many scenarios, they may not encompass all possibilities, leaving room for future expansion. To encourage community contributions, we provide both a Zenodo link to the current version and an public GitHub repository for active contribution.

The current version of the tool supports surface exposure and radiocarbon dating as well as any other form of dating as long as age ranges can be numerically quantified but it does not account for undated yet mapped landforms, such as moraines without ages. While we recognise the potential value of undated landforms for comparison with palaeoglacier simulations, it is challenging to integrate them into an automated, objective and quantitative framework like GLAMODAT.

In addition to the findings from the synthetic case presented above, additional insights could be gained from the real-world case study (cf. Appendix A), which helped to confirm the usability of the automatic calculation of the final misfit score. In this case, GLAMODAT was used for efficient and quantitative ensemble evaluation, as well as for adaptive exploration of the parameter space, whereby earlier runs are utilised to identify the areas with the greatest potential for improvement. However, we also note that a final misfit score as a single number may be ambiguous for various reasons (glaciers that are too short or too long or both for different periods). We therefore continue to see a benefit in examining specific maps of glacier history and individual misfit distances between model and data (as illustrated in the the glacier map Figures C2 and A5). Furthermore, we have found in the real-world case study that multiple different parameter configurations can lead to similarly well-fitting results (misfit distance < 500 m), which means that even a quantitative tool for data-model comparison in transient mode cannot

https://doi.org/10.5194/egusphere-2026-5635
Preprint. Discussion started: 6 November 2026
© Author(s) 2026. CC BY 4.0 License.

eliminate the ambiguity of the parameter space.

Ultimately, major improvements arise from the ability to model glaciers in large domains constrained by the geological record using GLAMODAT. First, glacier modelling can integrate rich datasets of glacier positions from thousands of studies. Second, it provides continuous reconstructions in space and time, offering insights in both data-rich and data-sparse regions. Third, the reconstructed glacier history may help refine climate reconstructions, addressing the limitations of single-location proxy records in temporal and spatial coverage. In summary, GLAMODAT improves how we can use geomorphological and geochronological data in palaeoglacier simulations which again improves the understanding of the complex interplay between past climate, past glacier extent and their mappable and datable records in the field.

5 Conclusions

This study presents a novel automated model-data comparison tool (GLAMODAT) designed to objectively evaluate model simulations of palaeoglaciers against empirical glacio-geomorphological and geochronological evidence. The tool reads results from ice-dynamical glacier evolution models and compares it to dated constraints on glacier history. It therein considers four palaeoglaciological categories: ice margin, ice free, ice cover and bedrock exposure. Using these context categories, GLAMODAT can handle comparisons despite complex palaeoglacier evolution scenarios involving multiple phases of advance and retreat.

GLAMODAT enables efficient and automated evaluation of glacier model performance and thereby provides the possibility for adaptive parameter exploration to find the best fitting glacier reconstruction. We evaluated its performance on glaciers in the European Alps with synthetically generated ages that exactly match the modelling reconstruction (Section 3) and further illustrate its performance on real-world catchment which also includes an example of automatic parameter optimisation (Section A).

GLAMODAT requires geomorphological and geochronological input data (structured like in Table D1 and categorised in four palaeoglaciological contexts) together with glacier model simulations results provided in a regular grid. The tool then automatically evaluates model simulations against the empirical evidence, producing individual mismatch distances for each age and a final misfit score for each run. GLAMODAT is distributed as open-source Python code, including a framework for adaptive parameter space exploration.

We envision GLAMODAT being applied to glacier simulations of multiple valleys or even whole mountain ranges, over large timescales of thousands of years, and for analysing ensemble runs and parameter optimisations. The best-performing simulations will produce a regional glacier history that aligns as best as possible with the available geomorphological and geochronological record. It could also be used to test new model representation of processes such as basal sliding, surface

https://doi.org/10.5194/egusphere-2026-5635
Preprint. Discussion started: 6 November 2026
© Author(s) 2026. CC BY 4.0 License.

mass balance, or ice flow. GLAMODAT has the potential to effectively quantify the fit of glacier simulations to the geological record. This makes it a valuable resource for assessing model results, conducting extended parameter studies and producing glacier model simulations that fit the empirical observations as best as possible.

Code availability. The GLAMODAT model-data comparison tool for transient palaeoglacier simulations is archived in Zenodo but also, intended for active further developments hosted on the github account (https://github.com/HenzAndreas/glamodat). The specific GLAMODAT code, IGM version 3.1, scripts for running and plotting for this publication are all archived here: https://doi.org/10.5281/zenodo.22795409 (Henz et al., 2026). The general link to the IGM glacier model is igm-model.org (last accessed 08.09.2026).

Data availability. All data for modelling besides the climate to reproduce the synthetic test case and the real-world case are uploaded to Zenodo (https://doi.org/10.5281/zenodo.22795409). Climate data can be downloaded from the original sources (Karger et al., 2020) and need reprojection to the model's coordinate system. We provide the scripts that are necessary to download the data together with the code on Zenodo (Henz et al., 2026). The AlpIce-1 database used for the real-world case study is provided by Kamleitner et al. (2026a)

Video supplement. For Fig. C2 and A5, we provide a full video of the glacier history for this simulations which are also archived on Zenodo https://doi.org/10.5281/zenodo.22795409.

https://doi.org/10.5194/egusphere-2026-5635
Preprint. Discussion started: 6 November 2026
© Author(s) 2026. CC BY 4.0 License.

Appendix A: Real-world case study in Central Switzerland

A1 Study site and data input

We present a case study from the Susten region (Sustenhorn: N 46.69, E 8.45, Fig. A1) in the Central Swiss Alps to demonstrate the full analysis and utility of GLAMODAT in conjunction with the AlpIce-1 database (Kamleitner et al., 2026b) and IGM glacier simulations (Jouvet et al., 2021). We present here an ensemble of 201 model runs that explore a parameter space for three climate parameters in an adaptive search for the optimal parameter combination.

The Susten region spans an elevation range from 700 to 3500 m a.s.l. and currently receives annual precipitation exceeding 2000 mm (MeteoSwiss, 2026). Its topography is characterised by the three main valleys of the Meiental, Gadmertal and Göscheneralptal, and many side valleys, steep upper sections, and elevated plateaus that remain glacierised today (Fig. A1). The palaeoglaciological history in the area is particularly well-studied, with a large number of dating records that provide detailed constraints on the YD and the Holocene glaciation history (Fig. A1 and Table D2, e.g., Schimmelpfennig et al., 2014; Boxleitner et al., 2017, 2019a, b)). Moreover, the presence of glaciers and palaeoglacier ages in both south- and north-facing side valleys likely represents a challenge for centre flowline modelling, highlighting the Susten region as a well suited case study for the application of a 3D glacier model with an automated model-data comparison approach. In summary, our comparison tool is tested in this region due to its diverse palaeoglaciological context and varied topography within a compact and extensively dated area.

The study region comprises of 53 event ages with high or medium confidence rating (Table D2; 45 ice margin, 7 ice free , 1 bedrock exposure context). We use these ages here only as summary event ages, which are sometimes points or associated with landforms, resulting from 31 events from surface exposure datings, 3 event ages from radiocarbon datings from the AlpIce database (Kamleitner et al., 2026b). To complement the AlpIce database, we include 19 LIA maximal glacier positions (lowest point in the glacier outlines by Reinthaler and Paul (2025) with areas larger than 1 km^2) and assigned age bounds of 1200-1870 CE, thus accounting for spatial spread during the LIA.

A2 Ensemble simulations

After defining the input database and model domain in time and space, we set up the ensemble runs for this real-world model-data comparison. For this, we first configured the study parameters and their intervals, followed by the selection of the sampling and optimisation algorithms. For simplifying the illustration of the comparison framework, we limit the ensemble model runs to vary three parameters related to mass balance forcing: an additive temperature offset correction, a multiplicative precipitation correction, and a process-based insolation correction for mass balance. The first two are parameters defined in increments of 0.1 (-2.0 to +1.0 for temperature and 0.5 to 2.0 for precipitation), while the aspect correction is a categorical choice of a dimensionless scaling factor with four options: no correction (0.0), two times moderate correction (0.75 and 0.9), and strong

https://doi.org/10.5194/egusphere-2026-5635
Preprint. Discussion started: 6 November 2026
© Author(s) 2026. CC BY 4.0 License.

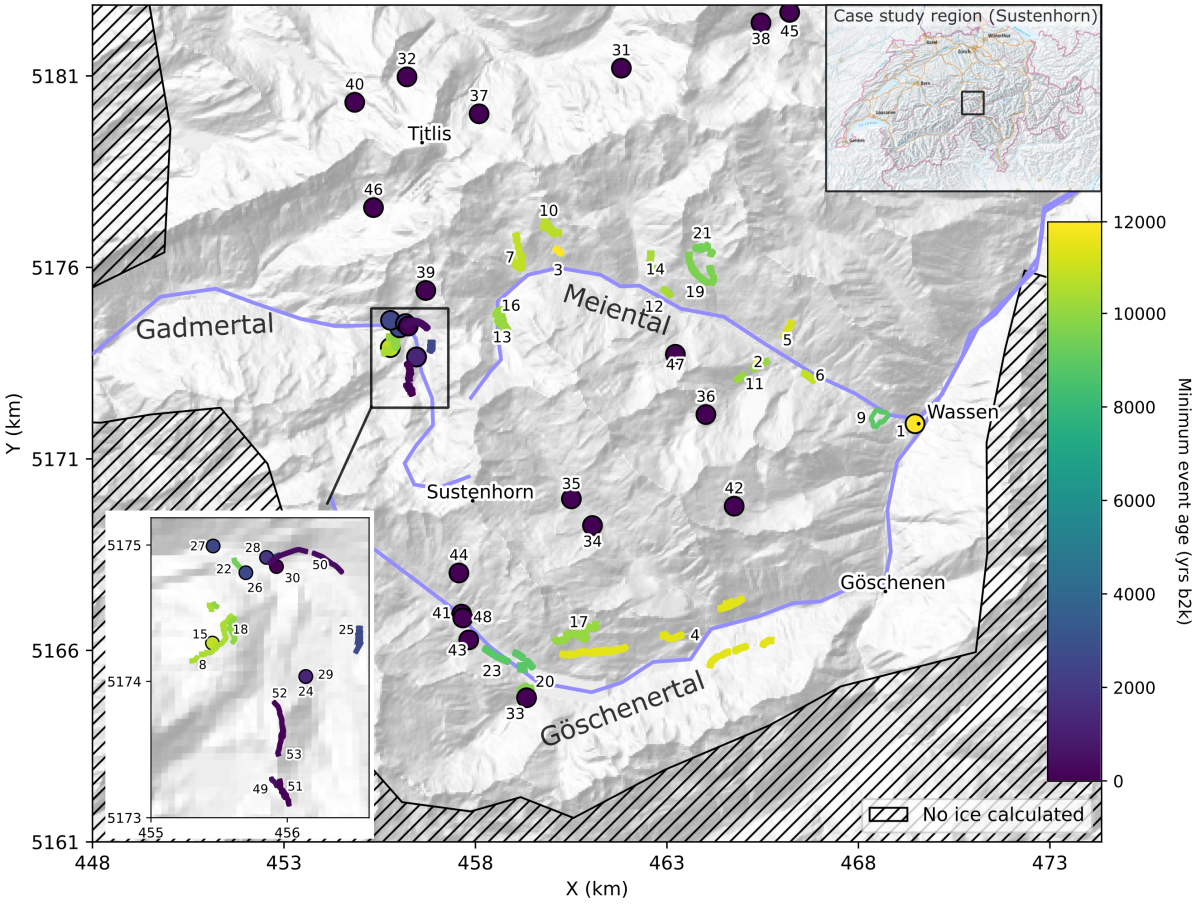


Figure A1. The case study region with all considered event ages in the model-data comparison tool. The region consists of 3 main valleys (Gadmertal, Meiental and Göschenertal) with a dense dating record. Inset figure shows very nearby points in Gadmertal (Region of Steingletscher today). Colours show the minimum age they have, due to reasons of readability we do not show the maximum age, so this is not showing the uncertainty in age. The full list with numbers and all important information is given in Appendix Table D2. Center flowlines to illustrate glacier length in Fig. A7 change over time in blue.

https://doi.org/10.5194/egusphere-2026-5635
Preprint. Discussion started: 6 November 2026
© Author(s) 2026. CC BY 4.0 License.

Table A1. Selected weighting parameters for the test-case and real-world glacier studies, used to combine single distances into an final misfit score. Weights account for elevation, confidence ratings, and data density to reflect their relative importance in the final score calculation.

Name	Value	Meaning
Elevation factor	10.0	Vertical distances weighted 10x
Confidence rating weights	high/medium: 1.0, low: 0.0	Equal weights to high and medium but excluding low confidence ratings
Data density	2.0	Sparse data (in time and space) are maximum weighted 2x a dating the in the most densely dated region

correction (1.5). The effect of these aspect corrections on the ELA is shown in Table B1. We conduct two separate phases of ensemble runs. The first 100 simulations use Sobol sampling for homogeneous exploration of the parameter space. Building on this ensemble, the second phase uses Random Forest Optimisation, guided by final misfit scores from the comparison tool GLAMODAT obtained from all previous model simulations. Each simulation is a full 15'000 year glacier model simulation at 50 m spatial resolution. In total, 201 simulations were performed, with one to five simulations running in parallel. The used weights for combining the single distances to a final misfit score are given in Table A1.

A3 Results and discussion of case study

The comparison tool automatically evaluates the ice extent in time and space for each of the 201 simulations against the 53 event ages. We visualise the misfit score of all event ages over time in Fig. A2. We also show four selected time frames in one of the best-performing simulations (293 m horizontal and 45 m vertical average misfit distance), where the glacier history is made visible. Additionally, the end-scores for all parameter sets are documented in Fig. A3 in running order of the experiments. We typically refer to euclidean, horizontal, and vertical distances in the text, since these are more intuitive. However, the adaptive optimisation algorithm minimises the final misfit score, which is a weighted combination of these distances and the spatio-temporal density of the age (as described above). The simulations with the minimal euclidean distances are still also the simulations with the minimal final misfit score, though the latter depends slightly more on the vertical distance (Fig. A4).

The scoring tool reveals a distinct pattern in model performance: simulations perform best (smallest overall model–data misfit of 200-400 m horizontal distance and 40-80 m vertical distance) with the forcing curve with either higher temperatures and increased precipitation (+0.0 to +0.5 °C and about 1.8 x precipitation) or lower temperatures and reduced precipitation (-1.0 °C and about 1.2 x precipitation, Fig. A6). The optimal parameter sets (minimal mismatch), thus, form a diagonal trough-like structure. This through-like structure is more pronounced with an insolation correction factor of 0.75 or 0.9 instead of 0.0 or 1.5. The overall averaged distances provide a comprehensive overview of all simulations, while the tool also allows for detailed examination of individual runs using the distances of the individual ages, as demonstrated in the synthetic case study

https://doi.org/10.5194/egusphere-2026-5635
Preprint. Discussion started: 6 November 2026
© Author(s) 2026. CC BY 4.0 License.

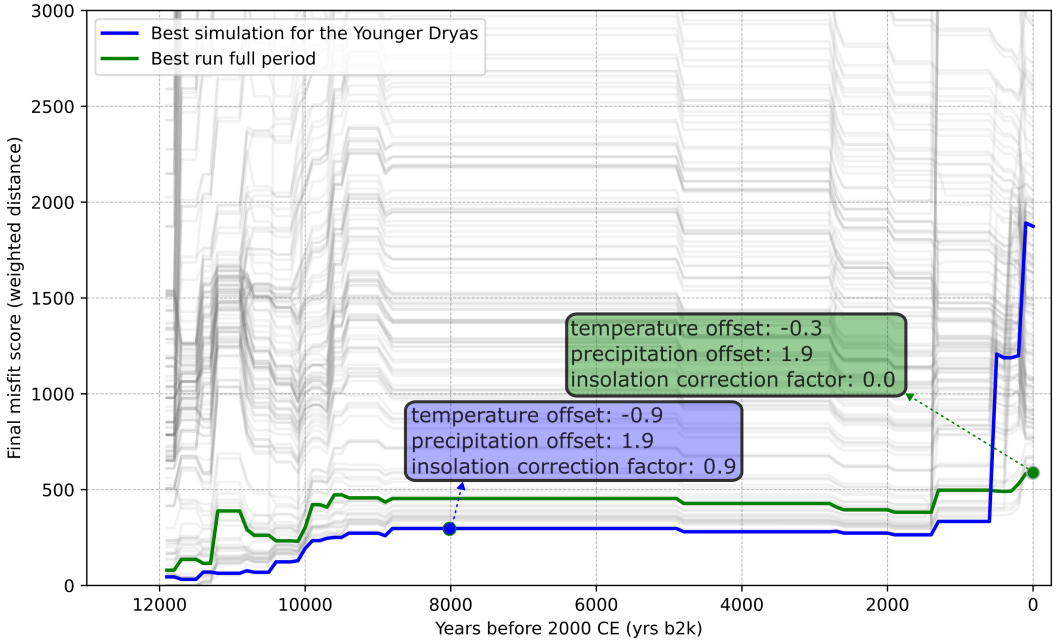


Figure A2. Averaged weighted final misfit score over time. All entries (ages and event ages) that can already be evaluated at a certain time step are averaged for a weighted distance over time. If the final misfit score increases, it indicates that new ages with a poorer model–data fit are contributing to the higher average, and vice versa. Different time periods may have simulations that perform better for one period than another (highlighted in blue and green lines).

(Section 3, Fig. 4).

When following the spatio-temporal evolution of the misfit over time (Fig. A5) we observe that many simulations that already perform well for the YD also achieve a final score below 2000. Glacier extent variations generally agree with the general glacier history that is known from Alps-wide interpretations (Fig. A7): a more extensive glacial phase during the Younger Dryas, a nearly deglaciated Early Holocene, and increasingly extensive glaciers towards the LIA (as suggested by many empirical studies, e.g., Ivy-Ochs et al., 1996; Boxleitner et al., 2019b). Therefore, we conclude that the climate input from Karger et al. (2020, 2023) produces within our data constraints an acceptable continuous glacial history throughout the Holocene.

Achieving perfect agreement (zero meter mismatch as an average) with the real-world data remains a challenge. We acknowledge that most of the problems with optimising glacier simulations to the data originate from the climate input and the model parameters for climate modifications, with the latter in our case remaining unchanged over time. Furthermore, we find that the 100-year climate snapshots used for the LIA advance are too coarse in terms of temporal resolution to reproduce the culmination of the LIA towards the end of this period. We believe that this is the reason why our LIA maximum in the simula-

https://doi.org/10.5194/egusphere-2026-5635
Preprint. Discussion started: 6 November 2026
© Author(s) 2026. CC BY 4.0 License.

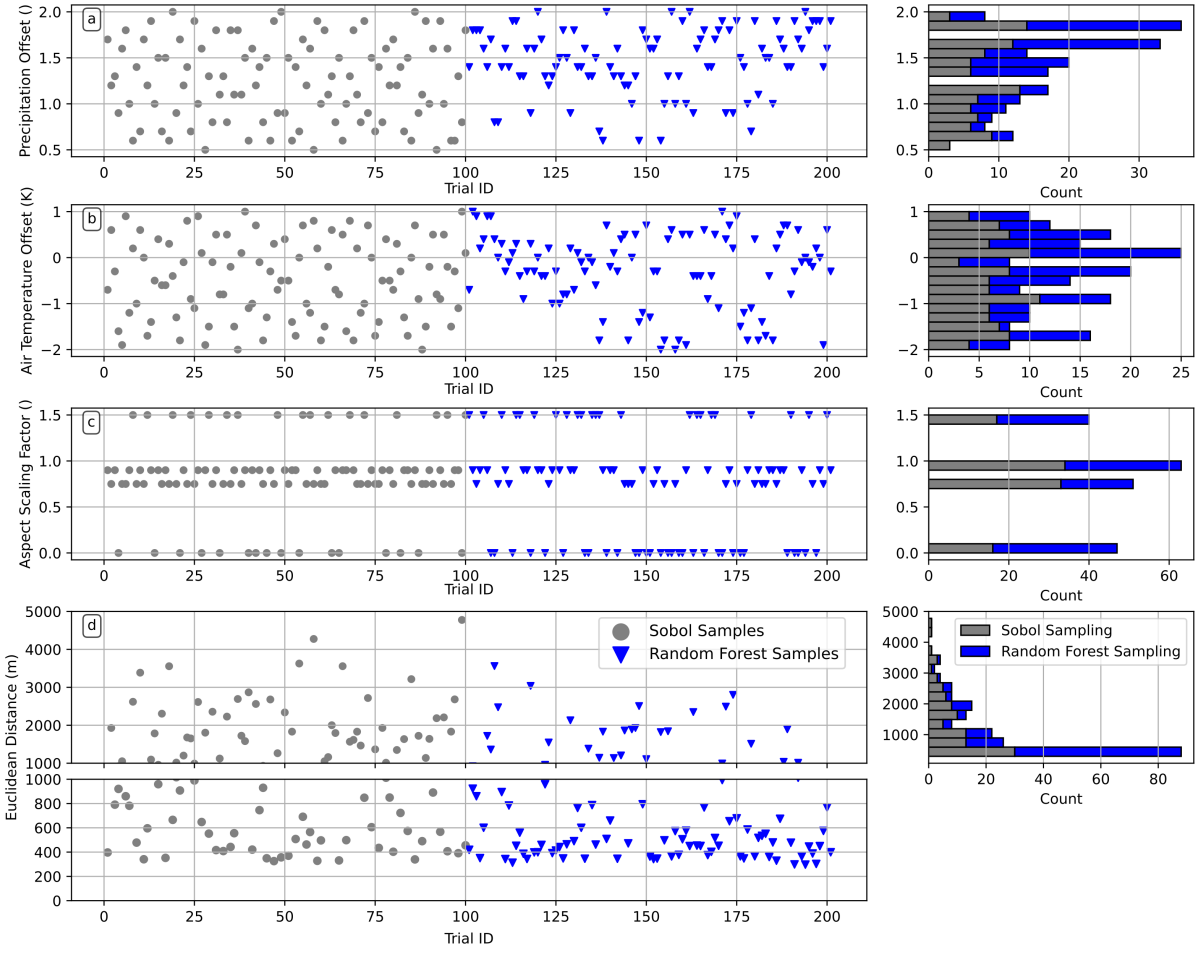


Figure A3. Parameter configurations for all individual ensemble simulations (Trial IDs). (a) Precipitation offset, applied as a multiplication factor to the 2D climate snapshot precipitation field. (b) Air temperature offset, applied as an additive offset to the 2D climate snapshot. (c) Aspect scaling factor, controlling the integration of solar radiation and accounting for higher temperatures in the ablation on south-facing grid cells. (d) Euclidean distance (averaged 3D distance to matching cell for all datings at the end of the model run), where zero would mean a full match. These are the true distances, not directly used for the optimisation. The relationship of the euclidean distance to the final misfit score is shown in Fig. A4.

tions generally occurs about 1000 years earlier than in historical records (Wanner et al., 2022). In addition, there are many more parameters that could be explored, including glacier-model parameters. Meanwhile, we obtain results below 350 m horizontal and vertical misfit distance for a range of parameter configurations, which we consider as an acceptable misfit. However, the range of simulation parameter combinations that reach this value highlights the difficulty of an under-defined problem where multiple parametrisations can produce equal model-data fits. We therefore still see value in looking into the specific runs and map-analyis for snapshots like as produced in our Figures 3 and A5. However, our results show that the tool successfully

https://doi.org/10.5194/egusphere-2026-5635
Preprint. Discussion started: 6 November 2026
© Author(s) 2026. CC BY 4.0 License.

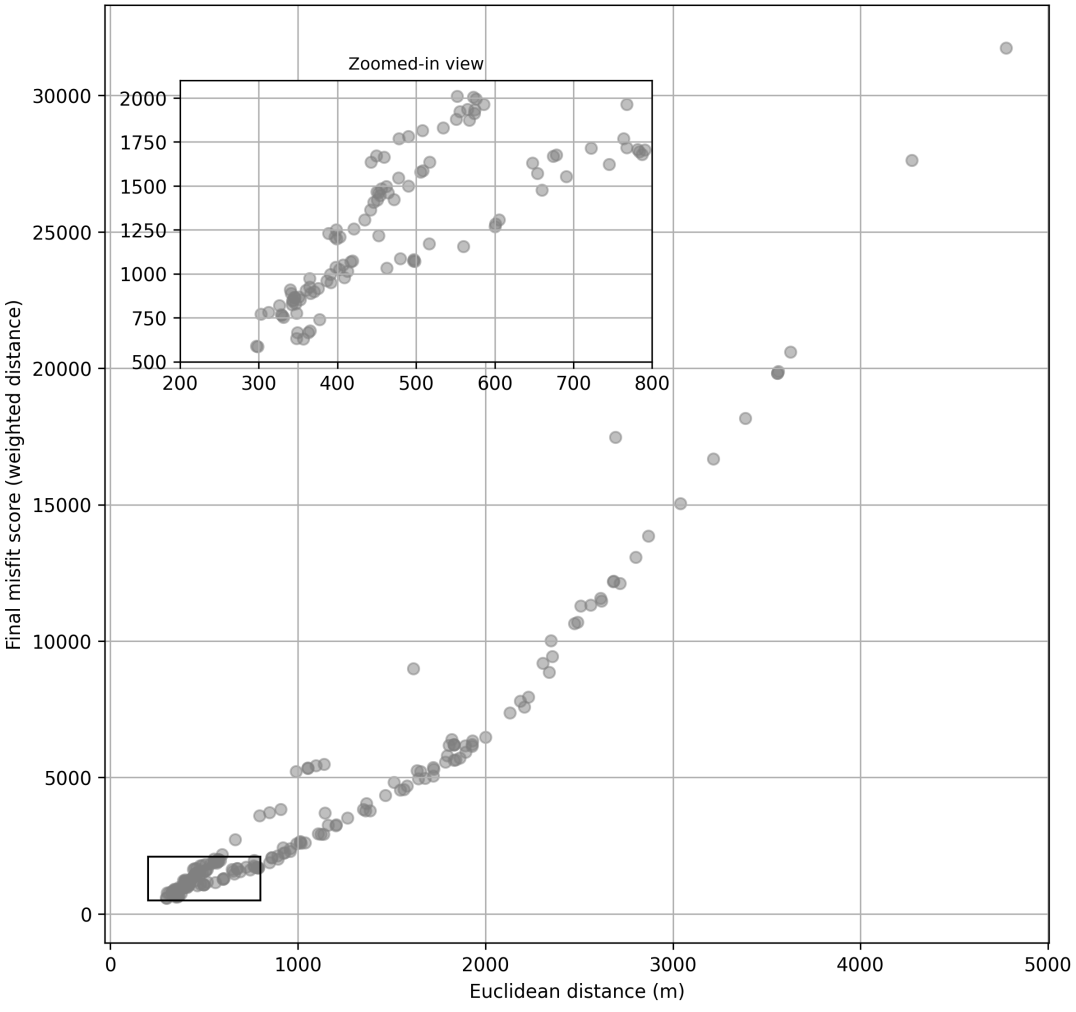


Figure A4. Final misfit score (used for parameter optimisation) versus actual euclidean misfit (average 3D distance to the next matching cell). The final misfit score is weighted based on the values in Table A1: vertical distance is weighted 10× more than horizontal distance, high and medium confidence ratings are treated equally, and spatio-temporally isolated ages are weighted up to 2× more than clustered ages. The illustration still shows that minimial final misfit for optimisation still means also a minimal average distance between the ages and a next matching cell in the glacier model output.

https://doi.org/10.5194/egusphere-2026-5635
Preprint. Discussion started: 6 November 2026
© Author(s) 2026. CC BY 4.0 License.

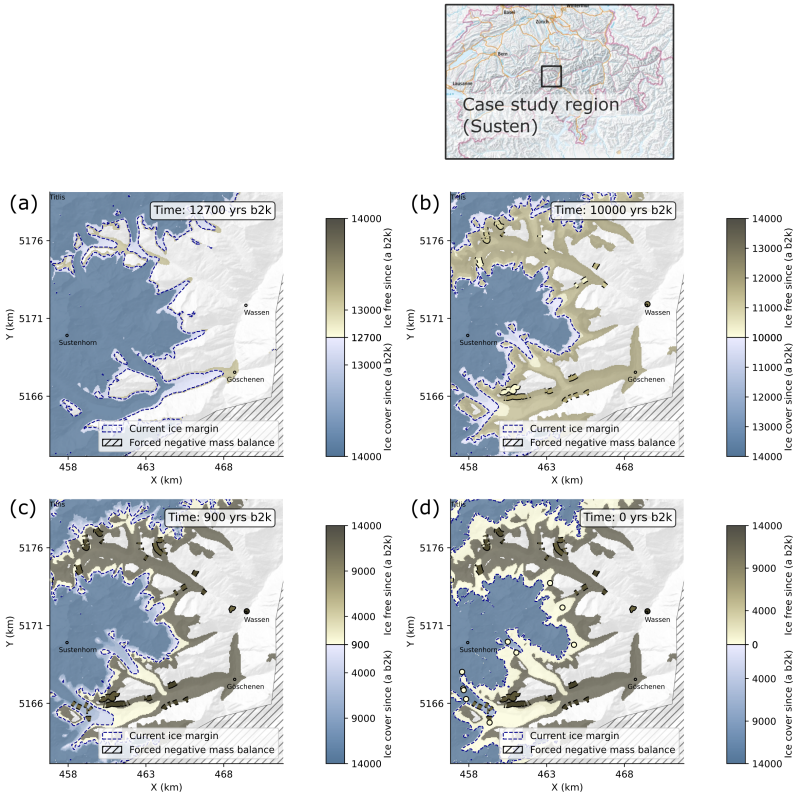


Figure A5. Glacier history of recently glaciated and ice-free regions, combined with event ages from the AlpIce database. Shown are four frames from one of the best-scoring simulations (green curve Fig. 4 with precipitation offset: 2.0; temperature offset and insolation correction factor: 0.0). The maps depict the east part of the study region with the current glacier extent, pixels continuously ice-covered since 14 ka b2k (before 2000 CE), and pixels ice-free since 14 ka b2k. (a) Light blue indicates recent glacier advances from the dark blue area (ice covered since 14 ka b2k). (b) At 10 ka b2k, the light brown footprint marks the former maximum extent (11–12 ka b2k), with recent smaller advances in light blue. Event ages are plotted at their minimum age: matching background colours indicate agreement; darker colours may suggest premature deglaciation (palaeocontext-dependent); lighter colours may indicate glaciers were too short (also palaeocontext-dependent). (c) Shortly before 900 a b2k, ochre shows a recent readvance and subsequent retreat phase, while bluish shades reveal smaller glaciers 1 to 4 ka earlier. (d) At 0 a b2k, the full glacier history is visible: the Younger Dryas (YD) footprint in dark brown, the 1000 a b2k advance in ochre, and Little Ice Age (LIA) event ages (ochre dots). Where ochre dots overlap blue areas, the modelled LIA extent is too large, whereas matches occur in ochre regions. A video of all timeframes of this glacier history is provided in the supplementary material. Temporary link for reviewers: https://drive.switch.ch/index.php/s/HlvwG9vdB8sKI4Q.

https://doi.org/10.5194/egusphere-2026-5635
Preprint. Discussion started: 6 November 2026
© Author(s) 2026. CC BY 4.0 License.

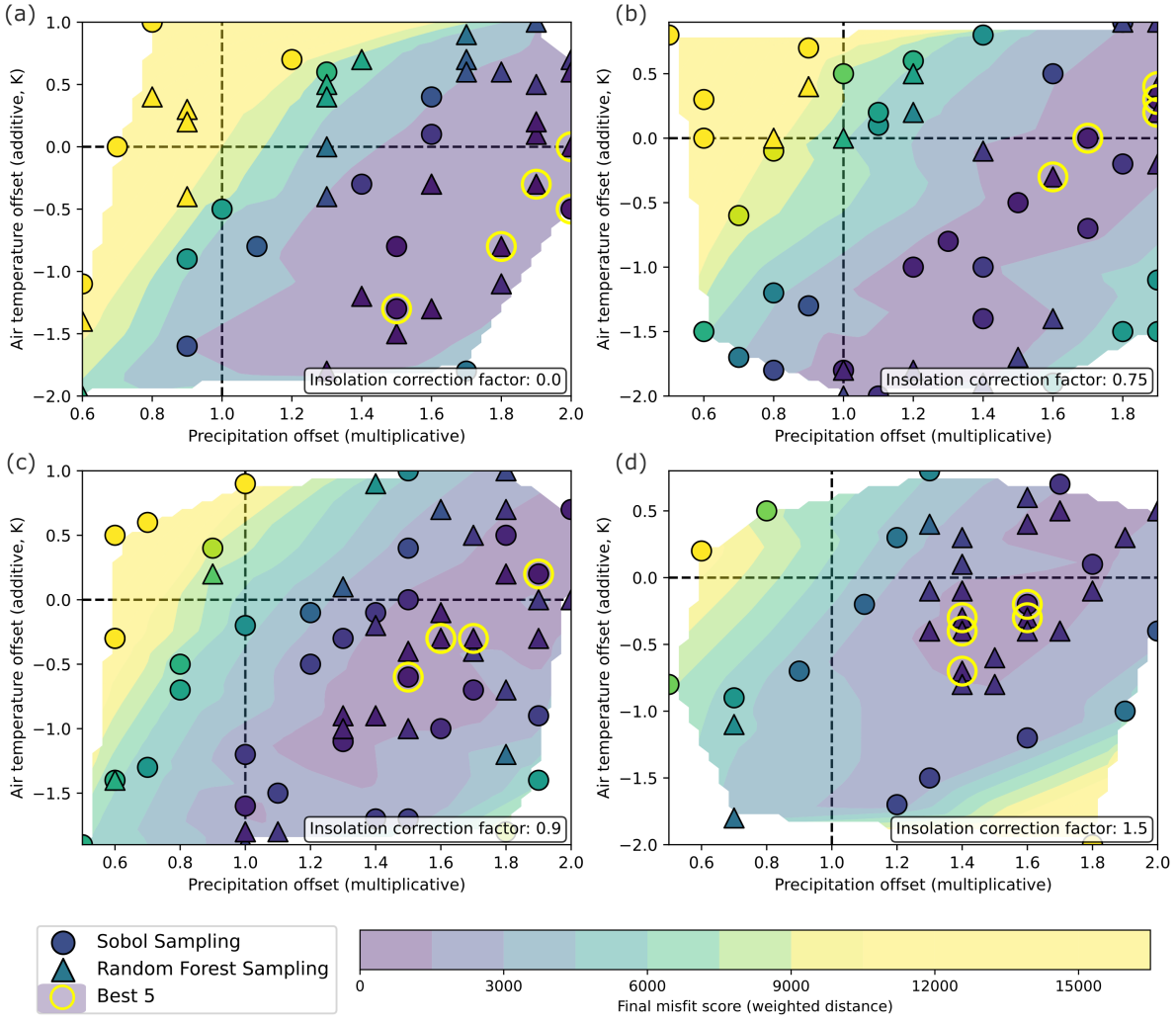


Figure A6. Weighted distance for all runs, evaluated until the final model time step at 0 b2k (2000 CE). The graph is split in the four chosen insolation correction factors 0.0 in (a) (no correction applied), 0.75 in (b), smaller insolation correction, 0.9 (b) bigger insolation correction and 1.5 (d) with the largest insolation correction. The only two other changed parameters, precipitation and temperature offsets, are shown on the two axis. The best five simulations each are marked with yellow circles.

differentiates between simulations that align closely with empirical evidence (< 350 m misfit on average) and those with large distance offsets (3000 m misfit on average). From a set of 201 simulations, we objectively identify the few best-fitting model simulations, hence the most acceptable modelling reconstruction that is continuous in space and time.

https://doi.org/10.5194/egusphere-2026-5635
Preprint. Discussion started: 6 November 2026
© Author(s) 2026. CC BY 4.0 License.

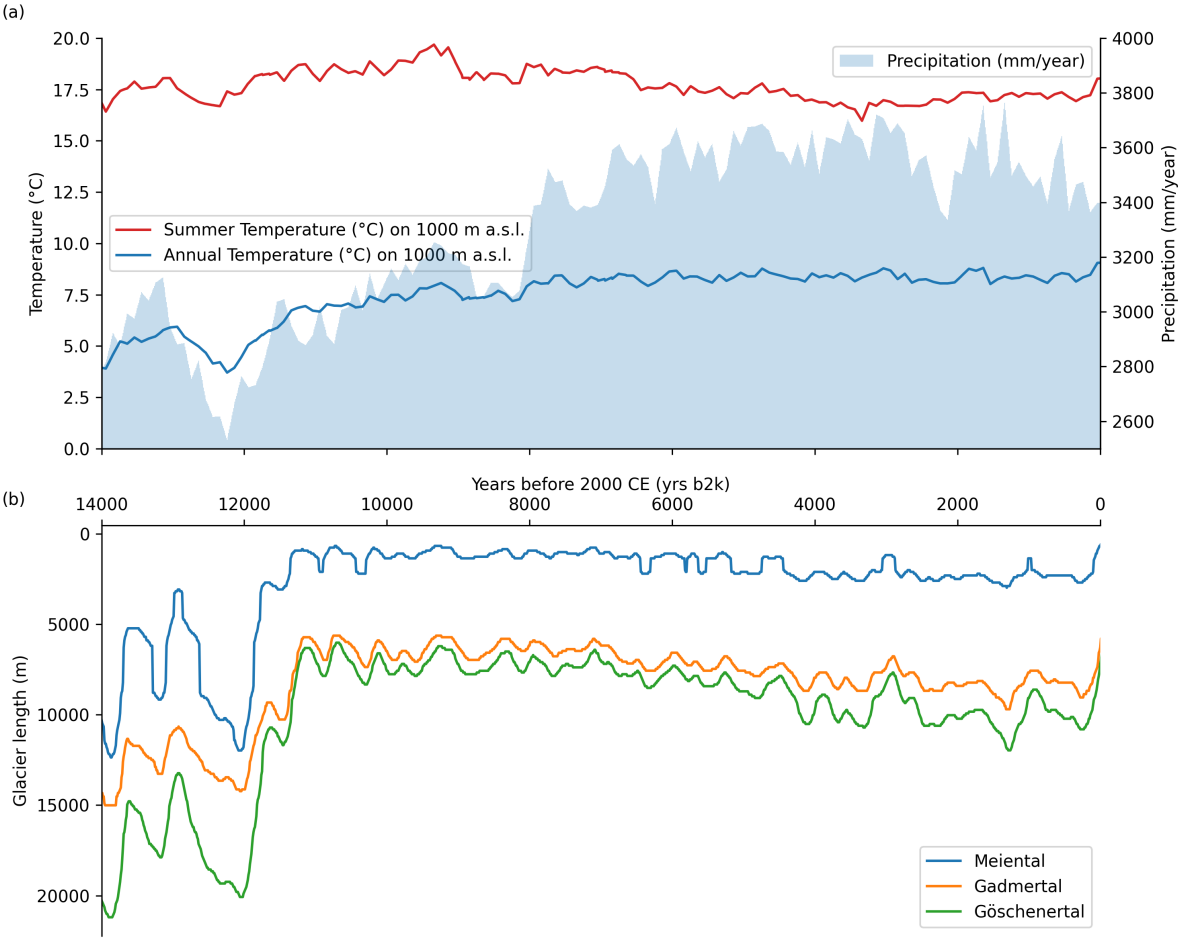


Figure A7. Climate (a) and glacier lengths (b) for the best scoring ensemble run in the case study region (simulation 194). (a) Climate values are already shown with the correction of 0.0 for temperature offset and 2.0 for precipitation offset. Distributed data in 1 km resolution is averaged over the modelling domain and corrected with an adiabatic lapse rate from the same dataset to 1000 m a.s.l. (CHELSA-TraCE21k Karger et al., 2023). (b) Glacier lengths over time calculated from hand-drawn glacier flowlines (see Fig. A1)

Appendix B: Surface mass balance correction factors for insolation

In this study, for glacier surface mass balance, we use a positive-degree-day (PDD) plus accumulation module (Hock, 2003, , implemented in IGM-3.1), enhanced by a correction factor for melt related to insolation, the latter of which is explained here.
445 We implemented a correction factor for solar insolation in the PDD scheme following and using the approach by Henz et al. (2025). Henz et al. (2025) already demonstrated that such a insolation based correction can provide a good estimate for mass balance adjustments on north- to south-facing valley glacier surfaces. We applied the insolation correction using a temperature offset based on the solar incidence angle, but only for the ablation calculation in the PDD framework. We do not change the

https://doi.org/10.5194/egusphere-2026-5635
Preprint. Discussion started: 6 November 2026
© Author(s) 2026. CC BY 4.0 License.

PDD scheme in the accumulation calculation because during precipitation phases, we observe little difference in the snowfall line within a single valley. We assume that precipitation and temperature differences between valleys are already incorporated in the gridded climate data input.

The correction method starts by first calculate a sun incidence angle for the midsummer sun for each grid cell. During summer in the European Alps, the sun is about 60° above the horizon, meaning a solar incidence angle of 30° corresponds to a flat surface (incidence angles are measured to the surface normal). The averaged latitude of the study region can be set as an input parameter. If the surface is exposed to the south (with a minimum possible incidence angle of 0.0°), we increase the temperature by the correction factor. If the surface is inclined at 30° towards the north, the incidence angle is 60°, and we subtract the correction factor from the temperature of that grid cell. Intermediate cases are linearly interpolated. To verify this approach, we calculated the mean Equilibrium Line Altitude (ELA) from the surface mass balance data field over the domain of the case-study area (Section A) for the the three specified bedrock slopes and expositions (Table B1). As a result, the ELA decreases for north-facing slopes and increases for south-facing slopes. Importantly, the correction has no effect on flat surfaces. With stronger correction factors, the ELA differences become larger (Table B1).

For this calculation of the mean ELA, we used the topography of the case-study region (Fig. A1) and the climate input from Karger et al. (2023, 2020) for the second-to-last time frame (corresponding to the calender years 1800 to 1899 CE). We applied a precipitation offset of 1.5 and a temperature offset of -1 K. The ELA was calculated by extracting the mean elevation of grid cells with a surface mass balance between -0.05 m and +0.05 m water equivalent.

Table B1. ELA values extracted from the case study topography using the given correction factor and sun incidence angle. The climate input corresponds to the second-to-last frame (meaning 1800-1899 CE, Karger et al., 2020), with precipitation and temperature offsets of 1.5 and -1.0 K, respectively.

insolation	sun incidence angle		
correction factor	0° (south facing)	30° (flat surface)	60° (north facing)
0.0	2610 m a.s.l.	2610 m a.s.l.	2610 m a.s.l.
0.75	2701 m a.s.l.	2610 m a.s.l.	2518 m a.s.l.
0.9	2719 m a.s.l.	2610 m a.s.l.	2500 m a.s.l.
1.5	2788 m a.s.l.	2610 m a.s.l.	2419 m a.s.l.

https://doi.org/10.5194/egusphere-2026-5635
Preprint. Discussion started: 6 November 2026
© Author(s) 2026. CC BY 4.0 License.

Appendix C: Appendix figures

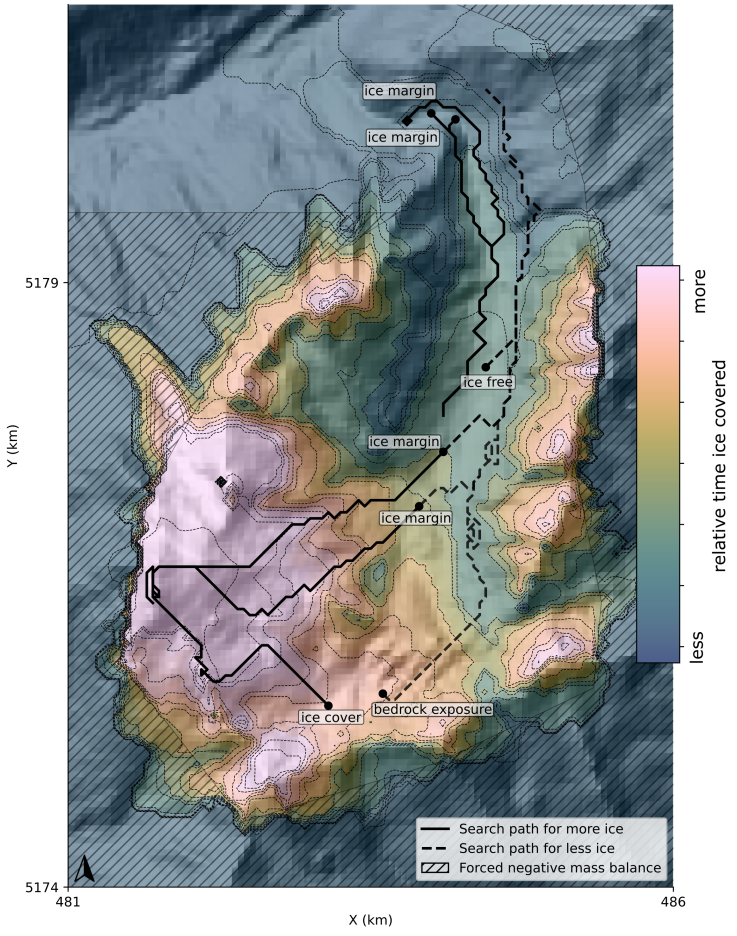


Figure C1. Illustration of the paths checked by the comparison tool to find matching cells based on glacier history (derived from the average of the three experiments A, B and C.). The search path depends on the palaeoglaciological category and status: for an ice margin, the tool checks for either reduced ice coverage (if currently ice-covered) or increased ice coverage (if currently ice-free); for an ice-cover age that is (in the model wrongly) ice free, it only searches toward more ice-covered conditions to find a next matching cell; for an ice-free ages, it searches toward reduced ice coverage. Search paths for ice margin ages that are ice free typically follow valley bottoms, tracing glacier tongues from upstream in the valley, while search paths for ice-free ages typically follow along valley sides, where ice retreat occurs earlier than at the valley floor (e.g. the valley sides are deglaciated earlier than a valley bottom of a larger glacier). This context-aware approach improves result interpretation by ensuring the search for matching cells aligns with the ages's context.

https://doi.org/10.5194/egusphere-2026-5635
Preprint. Discussion started: 6 November 2026
© Author(s) 2026. CC BY 4.0 License.

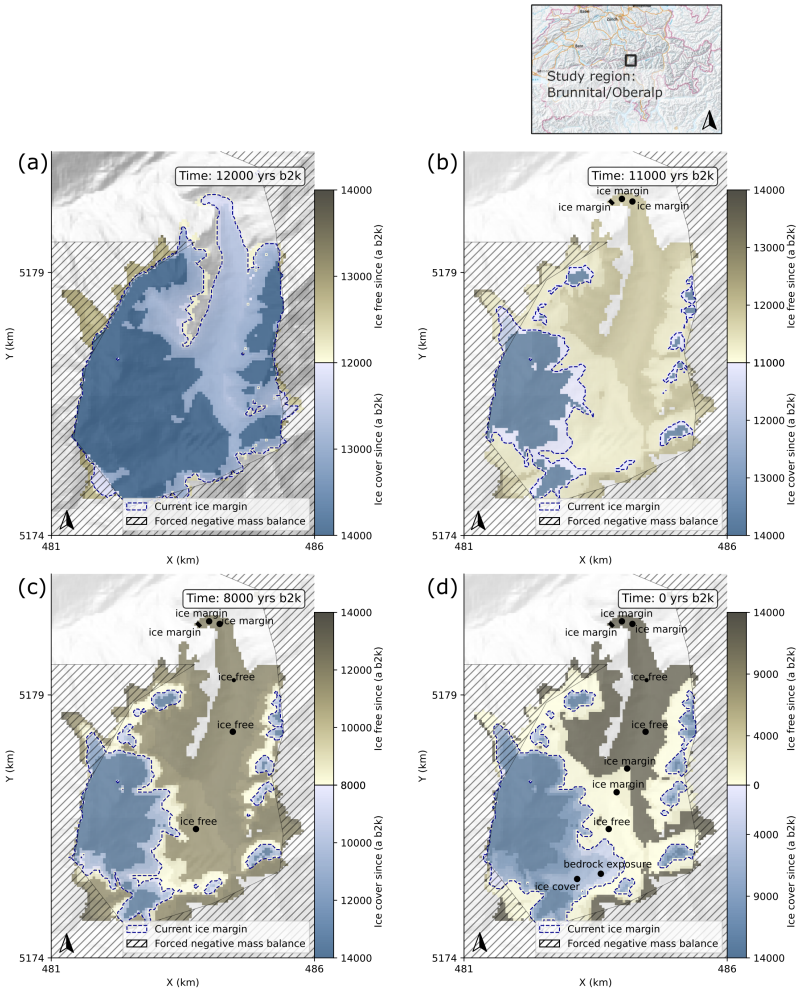


Figure C2. Glacier history of recently glaciated and ice-free regions, combined with fitting synthetic event ages generated from Experiment A (Tab 1). The maps depict the full study region with the glacier extent at the given time (top right of each plot given in years before 2000 CE (years b2k)). (a) Light blue indicates recent glacier advances from the dark blue area (ice-covered since 14 ka b2k). (b) At 11 ka b2k, the light brown footprint marks the former maximum extent (13-12 ka b2k), with recent smaller advances in light blue. Event ages are plotted at the time of their minimum age bound. (c) Shortly before 8000 ka b2k, ochre shows a recent advance and retreat, while dark bluish shades reveal smallest glaciers around 10 ka b2k. (d) At 0 a b2k (2000 CE), the full history is visible: the YD footprint in dark brown, the about 1000 ka b2k advance in ochre (LIA extents). A video of all time frames of this glacier history will is provided in the video supplement. Temporary link for reviewers: https://drive.switch.ch/index.php/s/HlvwG9vdB8sKI4Q.

Appendix D: Appendix tables

https://doi.org/10.5194/egusphere-2026-5635
Preprint. Discussion started: 6 November 2026
© Author(s) 2026. CC BY 4.0 License.

Table D1. Expected format of the input database with necessary columns names of the shapefiles. The table specifies the mandatory and optional fields for different types of input data (TCN datings, C14 datings, C14 event ages, and point event ages plus event ages with attributed landform geometries), with fields marked with an asterisk (*) being optional. As shapefiles are typically saved by single geometry type, multiple GIS shapefiles (e.g., points for ages, lines for moraine ridges, or polygons for rockfall footprints) are expected. Column names are taken unchanged from AlpIce-1 database and we refer to this database and publication for in-depth explanations what type of data is categorised in which palaeoglaciological context class (Kamleitner et al., 2026b).

Points with symmetric error	Points with age uncertainty range	Geometries with spatial extent and possible asymmetric error	Description	type/allowed values
Type of age				
TCN samples	C14, C14 event ages, point event ages	landform event ages		
Information and context				
geometry (points)	geometry (points)	geometry (points, lines, polygons)	Typical shapefile geometry column, where coordinates are saved (automatically generated when with a shapefile export from any GIS software)	array: coordinates, automatically produced by GIS software
date_ID or site_ID	date_ID or site_ID	date_ID or site_ID	Unique ID used for saving. Only one of both need to be present, if both are present, date_ID is preferred as it is more specific	string
confid_ra	confid_ra	confid_ra or confid_no	Confidence rating. Some event ages can come from multiple individual samples and ratings, where numbers give how many of each (confid_no)	string: high, medium, low
pc_cat	pc_cat	pc_cat	Palaeoglaciological context classification	string: ice free, ice margin, ice cover, bedrock exposure, ambiguous
pc_time	pc_time	pc_time	Subtype of ice-free context, if not given, long-term deglaciation is assumed	string: long-term deglaciation, ice-free interval or -
pc_subcat *	pc_subcat *	pc_subcat *	subtype of the ice free context, refering to stratigraphic setting, not directly used in the tool, only for plotting and context	string: ice advance, ice retreat, or ice retreat/readvance or -
Age				
r_exp_age, r_ext_err	recalc_max or e_age_max, recalc_min or e_age_min	e_age, e_ext_err or e_pos_err, e_neg_err	Name is different depending on type: symmetric age uncertainty (e.g. TCN dating), asymmetric errors (i.e. from event age calculation with positive and negative errors), min-max confidence interval (i.e. C14 ages)	numbers
Year of sampling or publication				
sample_yr or public_yr		mean_s_yr or mean_p_yr	For C14 and C14 event ages, years are commonly in Before Present (BP, before 1950), for others just in ages since sampling or age since publication if sampling is not given	numbers

https://doi.org/10.5194/egusphere-2026-5635
Preprint. Discussion started: 6 November 2026
© Author(s) 2026. CC BY 4.0 License.

Table D2. Event ages as used in the case study on the Susten region (see also Fig A1). Events are taken from the event age geometries database provided by Kamleitner et al. (2026a). In addition, we have added the known terminal positions of the glaciers from the LIA contours, where stars (*) are marked, the data was taken from Reinthaler and Paul (2025). The weight is the spatio-temporal weight applied to this age using the spatio-temporal weight factor of 2 based on the spatio-temporal uniqueness of this age (description in Section 2.6).

Index	ID	Original reference	palaeglaciologcial category	Subcategory	Time persepective	Type of age	Min_age	Max_age	Confidence rating	midpoint	Geometry type	Weight
1	ERR-Boxleitner2019b-A	Boxleitner et al. (2019b)	ice free	ice retreat	long-term deglaciation	event_age_landform	11951	13831	medium	469653, 5172792	Point	0.03
2	ICEM-Boxleitner2019b-E	Boxleitner et al. (2019b)	ice margin			event_age_landform	11771	13671	medium	465556, 5174383	LineString	0.022
3	ICEM-Boxleitner2019b-T	Boxleitner et al. (2019b)	ice margin			event_age_landform	11901	13621	medium	460338, 5177300	LineString	0.025
4	ICEM-Boxleitner2017-A	Boxleitner et al. (2017)	ice margin			event_age_landform	11443	13353	high	463065, 5167119	MultiLineString	0.027
5	ICEM-Boxleitner2019b-D	Boxleitner et al. (2019b)	ice margin			event_age_landform	11221	13121	medium	466328, 5175245	LineString	0.025
6	ICEM-Boxleitner2019b-N	Boxleitner et al. (2019b)	ice margin			event_age_landform	10881	12621	medium	466882, 5174024	LineString	0.023
7	ICEM-Boxleitner2019b-P	Boxleitner et al. (2019b)	ice margin			event_age_landform	10881	12601	medium	459305, 5177137	MultiLineString	0.023
8	BED-Schimmelpfennig2022-A	Schimmelpfennig et al. (2022)	bedrock exposure			event_age_landform	10804	12424	high	455950, 5174780	Point	0.016
9	MM-Boxleitner2019b-A	Boxleitner et al. (2019b)	ice free		long-term deglaciation	event_age_landform	8911	12311	medium	468704, 5172948	Polygon	0.021
10	ICEM-Boxleitner2019b-S	Boxleitner et al. (2019b)	ice margin			event_age_landform	10711	12261	high	460114, 5177895	MultiLineString	0.02
11	ICEM-Boxleitner2019b-F	Boxleitner et al. (2019b)	ice margin			event_age_landform	10111	11981	high	465447, 5174226	MultiLineString	0.018
12	ICEM-Boxleitner2019b-K	Boxleitner et al. (2019b)	ice margin			event_age_landform	10411	11971	medium	463005, 5176606	MultiLineString	0.018
13	ICEM-Boxleitner2019b-V	Boxleitner et al. (2019b)	ice margin			event_age_landform	10081	11801	medium	458867, 5175321	LineString	0.018
14	ICEM-Boxleitner2019b-J	Boxleitner et al. (2019b)	ice margin			event_age_landform	9921	11801	medium	462869, 5176804	LineString	0.018
15	ICEM-Schimmelpfennig2014-A	Schimmelpfennig et al. (2014)	ice margin			event_age_landform	10450	11650	high	455988, 5174832	MultiLineString	0.016
16	ICEM-Boxleitner2019b-U	Boxleitner et al. (2019b)	ice margin			event_age_landform	10131	11571	medium	458874, 5175533	MultiLineString	0.018
17	ICEM-Boxleitner2019a-A	Boxleitner et al. (2019a)	ice margin			event_age_landform	10081	11301	medium	460868, 5167292	MultiLineString	0.021
18	ICEM-Schimmelpfennig2014-B	Schimmelpfennig et al. (2014)	ice margin			event_age_landform	9950	11190	high	456084, 5174900	MultiLineString	0.016
19	ICEM-Boxleitner2019b-M	Boxleitner et al. (2019b)	ice margin			event_age_landform	9611	11051	medium	463987, 5176791	MultiLineString	0.02
20	ICEM-Boxleitner2019a-B	Boxleitner et al. (2019a)	ice margin			event_age_landform	9761	11021	medium	459478, 5165887	MultiLineString	0.018
21	ICEM-Boxleitner2019b-O	Boxleitner et al. (2019b)	ice margin			event_age_landform	9431	10851	medium	464088, 5177381	MultiLineString	0.021
22	ICEM-Schimmelpfennig2014-C	Schimmelpfennig et al. (2014)	ice margin			event_age_landform	9400	10670	high	456142, 5175344	LineString	0.016
23	ICEM-Boxleitner2019a-C	Boxleitner et al. (2019a)	ice margin			event_age_landform	8871	10471	medium	459075, 5166660	MultiLineString	0.029
24	14C-140-4	Hormes et al. (2006)	ice free		ice-free interval	event_age	4870	5320	medium	456635, 5174535	Point	0.028
25	ICEM-Schimmelpfennig2014-D	Schimmelpfennig et al. (2014)	ice margin			event_age_landform	2770	3090	high	456878, 5174952	MultiLineString	0.02
26	ERR-Schimmelpfennig2014-A	Schimmelpfennig et al. (2014)	ice free	ice retreat	long-term deglaciation	event_age_landform	2750	3070	high	456196, 5175296	Point	0.018
27	PROGL-Schimmelpfennig2014-A	Schimmelpfennig et al. (2014)	ice free		long-term deglaciation	event_age_landform	2640	2970	high	455956, 5175492	Point	0.019
28	14C-166-10	King (1974); Schimmelpfennig et al. (2014)	ice free		long-term deglaciation	event_age	1980	2520	medium	456347, 5175409	Point	0.019
29	14C-140-3	Hormes et al. (2006)	ice free		ice-free interval	event_age	1350	1450	medium	456635, 5174535	Point	0.017
30	lia_id_3337	Maisch et al. (2000)*	ice margin			event_age	130	800	high	456420, 5175342	Point	0.015
31	lia_id_3350	Maisch et al. (2000)*	ice margin			event_age	130	800	high	461985, 5182077	Point	0.018
32	lia_id_3309	Maisch et al. (2000)*	ice margin			event_age	130	800	high	456386, 5181849	Point	0.018
33	lia_id_2681	Maisch et al. (2000)*	ice margin			event_age	130	800	high	459509, 5165638	Point	0.016
34	lia_id_4294	Reinthaler and Paul (2025)	ice margin			event_age	130	800	high	461230, 5170136	Point	0.017
35	lia_id_3331	Maisch et al. (2000)*	ice margin			event_age	130	800	high	460679, 5170831	Point	0.017
36	lia_id_3372	Maisch et al. (2000)*	ice margin			event_age	130	800	high	464192, 5173033	Point	0.018
37	lia_id_3312	Maisch et al. (2000)*	ice margin			event_age	130	800	high	458270, 5180884	Point	0.018
38	lia_id_3347	Maisch et al. (2000)*	ice margin			event_age	130	800	high	465630, 5183259	Point	0.017
39	lia_id_3323	Maisch et al. (2000)*	ice margin			event_age	130	800	high	456877, 5176272	Point	0.017
40	lia_id_3311	Maisch et al. (2000)*	ice margin			event_age	130	800	high	455022, 5181184	Point	0.018
41	lia_id_3199	Maisch et al. (2000)*	ice margin			event_age	130	800	high	457813, 5167823	Point	0.016
42	lia_id_3373	Maisch et al. (2000)*	ice margin			event_age	130	800	high	464930, 5170639	Point	0.018
43	lia_id_2680	Maisch et al. (2000)*	ice margin			event_age	130	800	high	457999, 5167148	Point	0.016
44	lia_id_3334	Maisch et al. (2000)*	ice margin			event_age	130	800	high	457742, 5168895	Point	0.017
45	lia_id_3348	Maisch et al. (2000)*	ice margin			event_age	130	800	high	466379, 5183533	Point	0.017
46	lia_id_3316	Maisch et al. (2000)*	ice margin			event_age	130	800	high	455512, 5178435	Point	0.018
47	lia_id_3371	Maisch et al. (2000)*	ice margin			event_age	130	800	high	463395, 5174606	Point	0.018
48	lia_id_2676	Maisch et al. (2000)*	ice margin			event_age	130	800	high	457843, 5167722	Point	0.016
49	ICEM-Schimmelpfennig2014-H	Schimmelpfennig et al. (2014)	ice margin			event_age_landform	500	620	high	456433, 5173722	MultiLineString	0.016
50	ICEM-Schimmelpfennig2014-E	Schimmelpfennig et al. (2014)	ice margin			event_age_landform	460	560	high	456635, 5175408	MultiLineString	0.015
51	ICEM-Schimmelpfennig2014-I	Schimmelpfennig et al. (2014)	ice margin			event_age_landform	140	340	high	456475, 5173685	MultiLineString	0.016
52	ICEM-Schimmelpfennig2014-F	Schimmelpfennig et al. (2014)	ice margin			event_age_landform	260	320	high	456447, 5174159	LineString	0.015
53	ICEM-Schimmelpfennig2014-G	Schimmelpfennig et al. (2014)	ice margin			event_age_landform	180	200	high	456467, 5174111	MultiLineString	0.015

https://doi.org/10.5194/egusphere-2026-5635
Preprint. Discussion started: 6 November 2026
© Author(s) 2026. CC BY 4.0 License.

Author contributions. AH developed the main concept, led the preparation of the manuscript, designed the case studies and wrote the GLAMODAT code with methodological inputs from all authors. SK contributed domain expertise on the geomorphological and chronological framework of AlpIce-1 to support its correct integration into the comparison tool. All authors engaged in many constructive discussions on illustrations, argumentation lines and text. All authors gave extensive feedback before the submission of the manuscript.

Competing interests. The authors declare that they have no conflict of interest.

Acknowledgements. This research was part of the RECONCILE project and funded by the SNSF-Grant 200020_213077. A major part of the simulations was carried out on Octopus, a computing station at University of Lausanne (UNIL), which is managed by Ludovic Raess and supported by Guillaume Jouvet (UNIL). Parts of this script were drafted using AI writing tools (Mistral AI), and AI-assisted code completions were particularly helpful in generating the code lines for figures plus README files in the github repository (Github Copilot). Alessia Fransioli did all illustrative drawings (where mentioned in the figures) after input and initial drafts of AH.

https://doi.org/10.5194/egusphere-2026-5635
Preprint. Discussion started: 6 November 2026
© Author(s) 2026. CC BY 4.0 License.

References

Affolter, S., Häuselmann, A., Fleitmann, D., Edwards, R. L., Cheng, H., and Leuenberger, M.: Central Europe temperature constrained by speleothem fluid inclusion water isotopes over the past 14,000 years, Science Advances, 5, eaav3809, https://doi.org/10.1126/sciadv.aav3809, 2019.

Ahlmann, H. W.: Glaciers in Jotunheim and Their Physiography, Geografiska Annaler, 4, 1–57, https://doi.org/10.1080/20014422.1922.11881048, 1922.

Albrecht, T., Winkelmann, R., and Levermann, A.: Glacial-cycle simulations of the Antarctic Ice Sheet with the Parallel Ice Sheet Model (PISM) – Part 1: Boundary conditions and climatic forcing, The Cryosphere, 14, 599–632, https://doi.org/10.5194/tc-14-599-2020, 2020.

Alley, R. B., Mayewski, P. A., Sowers, T., Stuiver, M., Taylor, K. C., and Clark, P. U.: Holocene climatic instability: A prominent, widespread event 8200 yr ago, Geology, 25, 483–486, https://doi.org/10.1130/0091-7613(1997)025<0483:HCIAPW>2.3.CO;2, 1997.

Bette Otto-Bliesner, E., Tomas, R., Liu, Z., and He, C.: iTraCE, https://doi.org/10.26024/b290-an76, 2024.

Binaghi, M., Akçar, N., Ivy-Ochs, S., Yeşilyurt, S., Christl, M., and Schlüchter, C.: Lateglacial to Early Holocene glacier fluctuations in the northern Valaisian Alps, Swiss Journal of Geosciences, 118, 16, https://doi.org/10.1186/s00015-025-00486-7, 2025.

Boxleitner, M., Musso, A., Waroszewski, J., Malkiewicz, M., Maisch, M., Dahms, D., Brandová, D., Christl, M., de Castro Portes, R., and Egli, M.: Late Pleistocene – Holocene surface processes and landscape evolution in the central Swiss Alps, Geomorphology, 295, 306–322, https://doi.org/10.1016/j.geomorph.2017.07.006, 2017.

Boxleitner, M., Ivy-Ochs, S., Egli, M., Brandova, D., Christl, M., Dahms, D., and Maisch, M.: The 10Be deglaciation chronology of the Göschenertal, central Swiss Alps, and new insights into the Göschenen Cold Phases, Boreas, 48, 867–878, https://doi.org/10.1111/bor.12394, 2019a.

Boxleitner, M., Ivy-Ochs, S., Egli, M., Brandova, D., Christl, M., and Maisch, M.: Lateglacial and Early Holocene glacier stages - New dating evidence from the Meiental in central Switzerland, Geomorphology, 340, 15–31, https://doi.org/10.1016/j.geomorph.2019.04.004, 2019b.

Briggs, R. D. and Tarasov, L.: How to evaluate model-derived deglaciation chronologies: a case study using Antarctica, Quaternary Science Reviews, 63, 109–127, https://doi.org/10.1016/j.quascirev.2012.11.021, 2013.

Brown, V. H., Evans, D. J. A., Vieli, A., and Evans, I. S.: The Younger Dryas in the English Lake District: reconciling geomorphological evidence with numerical model outputs, Boreas, 42, 1022–1042, https://doi.org/10.1111/bor.12020, 2013.

Bueler, E. and Brown, J.: Shallow shelf approximation as a "sliding law" in a thermomechanically coupled ice sheet model, Journal of Geophysical Research, 114, https://doi.org/10.1029/2008JF001179, 2009.

Clark, C. D., Ely, J. C., Hindmarsh, R. C. A., Bradley, S., Ignéczi, A., Fabel, D., Ó Cofaigh, C., Chiverrell, R. C., Scourse, J., Benetti, S., Bradwell, T., Evans, D. J. A., Roberts, D. H., Burke, M., Callard, S. L., Medialdea, A., Saher, M., Small, D., Smedley, R. K., Gasson, E., Gregoire, L., Gandy, N., Hughes, A. L. C., Ballantyne, C., Bateman, M. D., Bigg, G. R., Doole, J., Dove, D., Duller, G. A. T., Jenkins, G. T. H., Livingstone, S. L., McCarron, S., Moreton, S., Pollard, D., Praeg, D., Sejrup, H. P., Van Landeghem, K. J. J., and Wilson, P.: Growth and retreat of the last British–Irish Ice Sheet, 31 000 to 15 000 years ago: the BRITICE-CHRONO reconstruction, Boreas, 51, 699–758, https://doi.org/10.1111/bor.12594, 2022.

Cohen, D., Gillet-Chaulet, F., Haeberli, W., Machguth, H., and Fischer, U. H.: Numerical reconstructions of the flow and basal conditions of the Rhine glacier, European Central Alps, at the Last Glacial Maximum, The Cryosphere, 12, 2515–2544, https://doi.org/10.5194/tc-12-2515-2018, 2018.

https://doi.org/10.5194/egusphere-2026-5635
Preprint. Discussion started: 6 November 2026
© Author(s) 2026. CC BY 4.0 License.

Cook, S. J., Jouvet, G., Millan, R., Rabatel, A., Zekollari, H., and Dussaillant, I.: Committed Ice Loss in the European Alps Until 2050 Using a Deep-Learning-Aided 3D Ice-Flow Model With Data Assimilation, Geophysical Research Letters, 50, e2023GL105 029, https://doi.org/10.1029/2023GL105029, 2023.

Davies, B. J., Darvill, C. M., Lovell, H., Bendle, J. M., Dowdeswell, J. A., Fabel, D., García, J.-L., Geiger, A., Glasser, N. F., Gheorghiu, D. M., Harrison, S., Hein, A. S., Kaplan, M. R., Martin, J. R. V., Mendelova, M., Palmer, A., Pelto, M., Rodés, A., Sagredo, E. A., Smedley, R. K., Smellie, J. L., and Thorndycraft, V. R.: The evolution of the Patagonian Ice Sheet from 35 ka to the present day (PATICE), Earth-Science Reviews, 204, 103 152, https://doi.org/10.1016/j.earscirev.2020.103152, 2020.

Ely, J. C., Clark, C. D., Small, D., and Hindmarsh, R. C. A.: ATAT 1.1, the Automated Timing Accordance Tool for comparing ice-sheet model output with geochronological data, Geoscientific Model Development, 12, 933–953, https://doi.org/10.5194/gmd-12-933-2019, 2019.

Frank, T., van Pelt, W. J. J., Rounce, D. R., Jouvet, G., and Hock, R.: Global glacier-free topography reveals a large potential for future lakes in presently ice-covered terrain, Nature Communications, 17, 3985, https://doi.org/10.1038/s41467-026-72548-9, 2026.

Golledge, N. R., Hubbard, A., and Sugden, D. E.: High-resolution numerical simulation of Younger Dryas glaciation in Scotland, Quaternary Science Reviews, 27, 888–904, https://doi.org/10.1016/j.quascirev.2008.01.019, 2008.

Greenwood, S. L. and Clark, C. D.: Subglacial bedforms of the Irish Ice Sheet, Journal of Maps, 4, 332–357, https://doi.org/10.4113/jom.2008.1030, 2008.

Henz, A., Reinthaler, J., Nussbaumer, S. U., Leger, T. P. M., Kamleitner, S., Jouvet, G., and Vieli, A.: Alps-wide high-resolution 3D modelling reconstruction of glacier geometry and climatic conditions for the Little Ice Age, The Cryosphere, 19, 5913–5937, https://doi.org/10.5194/tc-19-5913-2025, 2025.

Henz, A., Kamleitner, S., Nussbaumer, S., Leger, T., Jouvet, G., and Vieli, A.: GLAMODAT: a model-data comparison tool for assessing transient palaeoglacier simulations - code and data repository, https://doi.org/10.5281/zenodo.22795409, 2026.

Hock, R.: Temperature index melt modelling in mountain areas, Journal of Hydrology, 282, 104–115, https://doi.org/https://doi.org/10.1016/S0022-1694(03)00257-9, 2003.

Hock, R., Bliss, A., Marzeion, B., Giesen, R. H., Hirabayashi, Y., Huss, M., Radić, V., and Slangen, A. B. A.: GlacierMIP – A model intercomparison of global-scale glacier mass-balance models and projections, Journal of Glaciology, 65, 453–467, https://doi.org/10.1017/jog.2019.22, 2019.

Hormes, A., Beer, J., and Schlüchter, C.: A geochronological approach to understanding the role of solar activity on holocene glacier length variability in the swiss alps, Geografiska Annaler: Series A, Physical Geography, 88, 281–294, https://doi.org/10.1111/j.0435-3676.2006.00301.x, 2006.

Hughes, A. L., Clark, C. D., and Jordan, C. J.: Subglacial bedforms of the last British Ice Sheet, Journal of Maps, 6, 543–563, https://doi.org/10.4113/jom.2010.1111, 2010.

Hughes, A. L., Greenwood, S. L., and Clark, C. D.: Dating constraints on the last British-Irish Ice Sheet: a map and database, Journal of Maps, 7, 156–184, https://doi.org/10.4113/jom.2011.1145, 2011.

Ivy-Ochs, S., Schlüchter, C., Kubik, P., Synal, H.-A., Beer, J., and Kerschner, H.: The exposure age of an Egesen moraine at Julier Pass, Switzerland, measured with the cosmogenic radionuclides 10Be, 26A1 and 36Cl, Eclogae Geologicae Helvetiae, 89, 1049–1063, https://doi.org/10.5169/seals-893680, 1996.

Ivy-Ochs, S., Kerschner, H., Maisch, M., Christl, M., Kubik, P. W., and Schlüchter, C.: Latest Pleistocene and Holocene glacier variations in the European Alps, Quaternary Science Reviews, 28, 2137–2149, https://doi.org/10.1016/j.quascirev.2009.03.009, 2009.

https://doi.org/10.5194/egusphere-2026-5635
Preprint. Discussion started: 6 November 2026
© Author(s) 2026. CC BY 4.0 License.

Ivy-Ochs, S., Monegato, G., and Reitner, J. M.: Chapter 37 - The Alps: glacial landforms from the Bølling–Allerød Interstadial, in: European Glacial Landscapes, edited by Palacios, D., Hughes, P. D., García-Ruiz, J. M., and Andrés, N., pp. 355–360, Elsevier, ISBN 978-0-323-91899-2, https://doi.org/10.1016/B978-0-323-91899-2.00033-4, 2023a.

Ivy-Ochs, S., Monegato, G., and Reitner, J. M.: Chapter 55 - The Alps: glacial landforms from the Younger Dryas Stadial, in: European Glacial Landscapes, edited by Palacios, D., Hughes, P. D., García-Ruiz, J. M., and Andrés, N., pp. 525–539, Elsevier, ISBN 978-0-323-91899-2, https://doi.org/10.1016/B978-0-323-91899-2.00058-9, 2023b.

Jacquemart, M., Weber, S., Chiarle, M., Chmiel, M., Cicoira, A., Corona, C., Eckert, N., Gaume, J., Giacona, F., Hirschberg, J., Kaitna, R., Magnin, F., Mayer, S., Moos, C., van Herwijnen, A., and Stoffel, M.: Detecting the impact of climate change on alpine mass movements in observational records from the European Alps, Earth-Science Reviews, 258, 104 886, https://doi.org/10.1016/j.earscirev.2024.104886, 2024.

Japan Aerospace Exploration Agency: ALOS World 3D 30 meter DEM. V3.2, Jan 2021, https://doi.org/10.5069/G94M92HB, accessed: 2024-09-09, 2021.

Jouvet, G., Cordonnier, G., Kim, B., Lüthi, M., Vieli, A., and Aschwanden, A.: Deep learning speeds up ice flow modelling by several orders of magnitude, Journal of Glaciology, 68, 651–664, https://doi.org/10.1017/jog.2021.120, 2021.

Jouvet, G., Cohen, D., Russo, E., Buzan, J., Raible, C. C., Haeberli, W., Kamleitner, S., Ivy-Ochs, S., Imhof, M. A., Becker, J. K., Landgraf, A., and Fischer, U. H.: Coupled climate-glacier modelling of the last glaciation in the Alps, Journal of Glaciology, pp. 1–15, https://doi.org/10.1017/jog.2023.74, 2023.

Jouvet, G., Finley, B., Gregov, T., and Rosier, S.: IGM: an accessible, modular, differentiable, and GPU-accelerated high-order ice flow model, https://eartharxiv.org/repository/view/13712/, 2026.

Kamleitner, S., Ivy-Ochs, S., Leger, T., Henz, A., Nussbaumer, S., Vieli, A., and Jouvet, G.: AlpIce-1: A database of geochronological and geomorphological constraints on Alps-wide palaeoglacier fluctuations between the Last Glacial Maximum and the Holocene [Dataset], https://doi.org/10.5281/zenodo.21841122, in Boreas, 2026a.

Kamleitner, S., Ivy-Ochs, S., Leger, T. P. M., Henz, A., Nussbaumer, S. U., Vieli, A., and Jouvet, G.: AlpIce-1: a database of geochronological and geomorphological constraints on Alps-wide palaeoglacier fluctuations between the Last Glacial Maximum and the Holocene, Boreas, n/a, https://doi.org/10.1111/bor.70084, 2026b.

Karger, D. N., Nobis, M. P., Normand, S., Graham, C. H., and Zimmermann, N. E.: CHELSA-TraCE21k: Downscaled transient temperature and precipitation data since the last glacial maximum, https://doi.org/http://dx.doi.org/10.16904/envidat.211, 2020.

Karger, D. N., Nobis, M. P., Normand, S., Graham, C. H., and Zimmermann, N. E.: CHELSA-TraCE21k – high-resolution (1 km) downscaled transient temperature and precipitation data since the Last Glacial Maximum, Climate of the Past, 19, 439–456, https://doi.org/10.5194/cp-19-439-2023, 2023.

King, L.: Studien zur postglazialen Gletscher-und Vegetationsgeschichte des Sustenpassgebietes, 18, Schwabe Verlagsgruppe AG, https://www.buchfreund.de/de/d/p/77322368/studien-zur-postglazialen-gletscher-und, url accessed: 24.09.2026, 1974.

Le Roy, M., Ivy-Ochs, S., Nicolussi, K., Monegato, G., Reitner, J. M., Colucci, R. R., Ribolini, A., Spagnolo, M., and Stoffel, M.: Chapter 20: Holocene glacier variations in the Alps, European Glacial Landscapes: The Holocene, Elsevier, Amsterdam, https://doi.org/https://doi.org/10.1016/B978-0-323-99712-6.00018-0, 2024.

Lecavalier, B. S., Tarasov, L., Balco, G., Spector, P., Hillenbrand, C.-D., Buizert, C., Ritz, C., Leduc-Leballeur, M., Mulvaney, R., Whitehouse, P. L., Bentley, M. J., and Bamber, J.: Antarctic Ice Sheet paleo-constraint database, Earth System Science Data, 15, 3573–3596, https://doi.org/10.5194/essd-15-3573-2023, 2023.

https://doi.org/10.5194/egusphere-2026-5635
Preprint. Discussion started: 6 November 2026
© Author(s) 2026. CC BY 4.0 License.

Leger, T. P. M., Clark, C. D., Huynh, C., Jones, S., Ely, J. C., Bradley, S. L., Diemont, C., and Hughes, A. L. C.: A Greenland-wide empirical reconstruction of paleo ice sheet retreat informed by ice extent markers: PaleoGrIS version 1.0, Climate of the Past, 20, 701–755, https://doi.org/10.5194/cp-20-701-2024, 2024.

Leger, T. P. M., Ely, J. C., Clark, C. D., Bradley, S. L., Archer, R. E., and Zhu, J.: The Greenland-Ice-Sheet evolution over the last 24 000 years: insights from model simulations evaluated against ice-extent markers, The Cryosphere, 19, 5719–5761, https://doi.org/10.5194/tc-19-5719-2025, 2025a.

Leger, T. P. M., Jouvet, G., Kamleitner, S., Mey, J., Herman, F., Finley, B. D., Ivy-Ochs, S., Vieli, A., Henz, A., and Nussbaumer, S. U.: A data-consistent model of the last glaciation in the Alps achieved with physics-driven AI, Nature Communications, 16, 848, https://doi.org/10.1038/s41467-025-56168-3, 2025b.

Li, Y., Napieralski, J., Harbor, J., and Hubbard, A.: Identifying patterns of correspondence between modeled flow directions and field evidence: An automated flow direction analysis, Computers & Geosciences, 33, 141–150, https://doi.org/10.1016/j.cageo.2006.06.016, 2007.

Mackintosh, A. N., Anderson, B. M., and Pierrehumbert, R. T.: Reconstructing Climate from Glaciers, Annual Review of Earth and Planetary Sciences, 45, 649–680, https://doi.org/10.1146/annurev-earth-063016-020643, 2017.

Maisch, M., Wipf, A., Denneler, B., Battaglia, J., and Benz, C.: Die Gletscher der Schweizer Alpen: Gletscherhochstand 1850, aktuelle Vergletscherung, Gletscherschwundszenarien, Schlussbericht NFP 31, second edn., Hochschulverlag ETH Zurich, Zurich, Zürich, ISBN 3-7281-2733-7, https://www.researchgate.net/publication/292773621_Die_Gletscher_Der_Schweizer_Alpen_Gletscherhochstand_1850, url accessed: 24.09.2026, 2000.

Marzeion, B., Hock, R., Anderson, B., Bliss, A., Champollion, N., Fujita, K., Huss, M., Immerzeel, W. W., Kraaijenbrink, P., Malles, J.-H., Maussion, F., Radić, V., Rounce, D. R., Sakai, A., Shannon, S., van de Wal, R., and Zekollari, H.: Partitioning the Uncertainty of Ensemble Projections of Global Glacier Mass Change, Earth's Future, 8, https://doi.org/10.1029/2019EF001470, 2020.

MeteoSwiss: The climate of Switzerland - MeteoSwiss, https://www.meteoswiss.admin.ch/climate/the-climate-of-switzerland.html, last accessed: 27.05.2026, 2026.

Napieralski, J.: GIS and Field-Based Spatiotemporal Analysis for Evaluation of Paleo–Ice Sheet Simulations*, The Professional Geographer, 59, 173–183, https://doi.org/10.1111/j.1467-9272.2007.00605.x, 2007.

Napieralski, J., Li, Y., and Harbor, J.: Comparing predicted and observed spatial boundaries of geologic phenomena: Automated Proximity and Conformity Analysis applied to ice sheet reconstructions, Computers & Geosciences, 32, 124–134, https://doi.org/10.1016/j.cageo.2005.05.011, 2006.

Nesje, A. and Dahl, S. O.: Equilibrium-line altitude depressions of reconstructed Younger Dryas and Holocene glaciers in Fosdalen, inner Nordfjord, western Norway, Norsk Geologisk Tidsskrift, https://pascal-francis.inist.fr/vibad/index.php?action=getRecordDetail&idt=5567235, url accessed: 24.09.2026, 1992.

Oerlemans, J.: A flowline model for Nigardsbreen, Norway: projection of future glacier length based on dynamic calibration with the historic record, Annals of Glaciology, 24, 382–389, https://doi.org/10.3189/S0260305500012489, 1997.

Oerlemans, J.: Glaciers and climate change, Balkema Publishers, ISBN 978-1-003-76067-2, https://doi.org/10.1201/9781003760672, 2001.

Ohmura, A., Kasser, P., and Funk, M.: Climate at the Equilibrium Line of Glaciers, Journal of Glaciology, 38, 397–411, https://doi.org/10.3189/S0022143000002276, 1992.

Porter, S. C.: Equilibrium-line Altitudes of Late Quaternary Glaciers in the Southern Alps, New Zealand, Quaternary Research, 5, 27–47, https://doi.org/10.1016/0033-5894(75)90047-2, 1975.

https://doi.org/10.5194/egusphere-2026-5635
Preprint. Discussion started: 6 November 2026
© Author(s) 2026. CC BY 4.0 License.

Protin, M., Schimmelpfennig, I., Mugnier, J.-L., Ravanel, L., Le Roy, M., Deline, P., Favier, V., Buoncristiani, J.-F., Aumaître, G., Bourlès, D. L., and Keddadouche, K.: Climatic reconstruction for the Younger Dryas/Early Holocene transition and the Little Ice Age based on paleo-extents of Argentière glacier (French Alps), Quaternary Science Reviews, 221, 105 863, https://doi.org/10.1016/j.quascirev.2019.105863, 2019.

Reinthaler, J. and Paul, F.: Reconstructed glacier area and volume changes in the European Alps since the Little Ice Age, The Cryosphere, 19, 753–767, https://doi.org/10.5194/tc-19-753-2025, 2025.

Rounce, D. R., Khurana, T., Short, M. B., Hock, R., Shean, D. E., and Brinkerhoff, D. J.: Quantifying parameter uncertainty in a large-scale glacier evolution model using Bayesian inference: application to High Mountain Asia, Journal of Glaciology, 66, 175–187, https://doi.org/10.1017/jog.2019.91, 2020.

Rounce, D. R., Hock, R., Maussion, F., Hugonnet, R., Kochtitzky, W., Huss, M., Berthier, E., Brinkerhoff, D., Compagno, L., Copland, L., Farinotti, D., Menounos, B., and McNabb, R. W.: Global glacier change in the 21st century: Every increase in temperature matters, Science, 379, 78–83, https://doi.org/10.1126/science.abo1324, 2023.

Schimmelpfennig, I., Schaefer, J. M., Akçar, N., Koffman, T., Ivy-Ochs, S., Schwartz, R., Finkel, R. C., Zimmerman, S., and Schlüchter, C.: A chronology of Holocene and Little Ice Age glacier culminations of the Steingletscher, Central Alps, Switzerland, based on high-sensitivity beryllium-10 moraine dating, Earth and Planetary Science Letters, 393, 220–230, https://doi.org/10.1016/j.epsl.2014.02.046, 2014.

Schimmelpfennig, I., Schaefer, J. M., Lamp, J., Godard, V., Schwartz, R., Bard, E., Tuna, T., Akçar, N., Schlüchter, C., Zimmerman, S., and Team, A.: Glacier response to Holocene warmth inferred from in situ ^{10}Be and ^{14}C bedrock analyses in Steingletscher's forefield (central Swiss Alps), Climate of the Past, 18, 23–44, https://doi.org/10.5194/cp-18-23-2022, 2022.

Sissons, J. B.: A Late-Glacial Ice Cap in the Central Grampians, Scotland, Transactions of the Institute of British Geographers, pp. 95–114, https://doi.org/10.2307/621517, 1974.

Tarasov, L. and Peltier, W. R.: A geophysically constrained large ensemble analysis of the deglacial history of the North American ice-sheet complex, Quaternary Science Reviews, 23, 359–388, https://doi.org/10.1016/j.quascirev.2003.08.004, 2004.

Van Tricht, L., Zekollari, H., Huss, M., Rounce, D. R., Schuster, L., Aguayo, R., Schmitt, P., Maussion, F., Tober, B., and Farinotti, D.: Peak glacier extinction in the mid-twenty-first century, Nature Climate Change, 16, 143–147, https://doi.org/10.1038/s41558-025-02513-9, 2026.

von Scheffer, C., De Vleeschouwer, F., Le Roux, G., and Unkel, I.: From the 8.2 ka event to the Little Ice Age: Holocene cold periods and human impact recorded in alpine glaciofluvial peatlands (Silvretta Mountains, Switzerland), E&G Quaternary Science Journal, 74, 263–279, https://doi.org/10.5194/egqsj-74-263-2025, 2025.

Wanner, H., Pfister, C., and Neukom, R.: The variable European Little Ice Age, Quaternary Science Reviews, 287, 107 531, https://doi.org/10.1016/j.quascirev.2022.107531, 2022.

Zekollari, H., Huss, M., Farinotti, D., and Lhermitte, S.: Ice-Dynamical Glacier Evolution Modeling—A Review, Reviews of Geophysics, 60, e2021RG000 754, https://doi.org/10.1029/2021RG000754, 2022.

Zekollari, H., Schuster, L., Maussion, F., Hock, R., Marzeion, B., Rounce, D. R., Compagno, L., Fujita, K., Huss, M., James, M., Kraaijenbrink, P. D. A., Lipscomb, W. H., Minallah, S., Oberrauch, M., Van Tricht, L., Champollion, N., Edwards, T., Farinotti, D., Immerzeel, W., Leguy, G., and Sakai, A.: Glacier preservation doubled by limiting warming to 1.5°C versus 2.7°C, Science, 388, 979–983, https://doi.org/10.1126/science.adu4675, 2025.

https://doi.org/10.5194/egusphere-2026-5635
Preprint. Discussion started: 6 November 2026
© Author(s) 2026. CC BY 4.0 License.



Åkesson, H., Nisancioglu, K. H., Giesen, R. H., and Morlighem, M.: Simulating the evolution of Hardangerjøkulen ice cap in southern
670 Norway since the mid-Holocene and its sensitivity to climate change, The Cryosphere, 11, 281–302, https://doi.org/10.5194/tc-11-281-2017, 2017.